JOURNAL OF GEOPHYSICAL RESEARCH, VOL. 115, B07404, doi:10.1029/2009JB006417, 2010

GPS crustal deformation, strain rate, and seismic activity after the 1999 Chi-Chi earthquake in Taiwan

Kuan-Chuan Lin,[1,2] Jyr-Ching Hu,[1] Kuo-En Ching,[3] Jacques Angelier,[4] Ruey-Juin Rau,[3] Shui-Beih Yu,[5] Chun-Hsiung Tsai,[2] Tzay-Chyn Shin,[2] and Mong-Han Huang[1]

Received 14 March 2009; revised 10 December 2009; accepted 27 January 2010; published 13 July 2010.

[1] Using data at 110 continuous GPS stations from 1 January 2003 to 31 December 2005, we characterized the surface deformation in Taiwan after the M_w = 7.6 Chi-Chi earthquake of 21 September 1999. In continuous GPS (CGPS) data, the maximum coseismic deformation of the Chengkung earthquake and Ilan double earthquakes reached 165.5 ± 0.5 mm and 35.4 ± 0.5 mm in horizontal displacement and 181.7 ± 1.1 mm and 12.6 ± 1.5 mm in vertical displacement, respectively. With respect to Paisha station, S01R, the stations of the Coastal Range and Lanhsu showed an average displacement of 40.5–93.6 mm/yr with directions of 307°–333°. The stations in the Longitudinal Valley and Central Range revealed velocities in the range 19.0–49.3 mm/yr with directions of 285°–318°. In western Taiwan, the velocities in the inner fold-and-thrust belt range from 14.2 to 45.5 mm/yr with directions of 284°–304°. Extensional strain affects the Ilan and Pingtung plains near belt tips, revealing lateral extrusion toward the adjacent subduction zones. Extensional strain also affects the southern Central Range because of the rapid uplift related to the southward propagating collision process. Large and medium size earthquakes affect the strain pattern revealed by CGPS, albeit in different ways: regional extension and displacement were large and rotations were small regarding the M_w = 7.6 Chi-Chi earthquake. In contrast, the limited size of the affected area, moderate displacement, and large rotations characterized the 2003 M_w = 6.8 Chengkung earthquake. The impact of smaller earthquakes such as the 2005 M_w = 5.9 Ilan double earthquakes and the 2005 M_w = 5.6 Hualien earthquake was locally significant but regionally minor. The CGPS data provide a snapshot of the deformation that is generally consistent with the long-term history of the collision but should not be directly extrapolated because thrust deformation is migrating along the tectonic boundary. Regarding the Chi-Chi earthquake, the new CGPS data show that the Chi-Chi hanging wall is still recognizable as a kinematic block, whereas in the previous pattern the hanging wall was not discernable.

Citation: Lin, K.-C., J.-C. Hu, K.-E. Ching, J. Angelier, R.-J. Rau, S.-B. Yu, C.-H. Tsai, T.-C. Shin, and M.-H. Huang (2010), GPS crustal deformation, strain rate, and seismic activity after the 1999 Chi-Chi earthquake in Taiwan, *J. Geophys. Res.*, *115*, B07404, doi:10.1029/2009JB006417.

1. Introduction

[2] Along the convergent boundary between the South China Block of Eurasia and the Philippine Sea Plate (Figure 1), thousands of earthquakes hit Taiwan and its surroundings each year [*Tsai*, 1986; *Wang and Shin*, 1998]. The mountain belt of Taiwan [*Ho*, 1986] results from an oblique collision between the Luzon volcanic arc of the Philippine Sea Plate and the continental margin of the Eurasian Plate [*Suppe*, 1980, 1984]. The present-day convergent rate of the two plates was considered to be about 7.3 cm/yr in the N49°W direction [*Seno et al.*, 1993], but on the basis of geodetic GPS analyses, *Yu et al.* [1997, 1999] determined a faster rate, 8.2 cm/yr, consistent with recent plate tectonic models [*Zang et al.*, 2002]. The difference between these results is related to the displacement of south China with respect to Eurasia [*Angelier et al.*, 2000]. Plate convergence in this region produces the dominant driving force and stress concentration across the Taiwan mountain belt [*Hu et al.*, 1996, 2002].

[3] The Global Positioning System has become one of the most important geodetic tools for studying crustal defor-

[1]Department of Geosciences, National Taiwan University, Taipei, Taiwan.
[2]Seismological Observation Center, Central Weather Bureau, Taipei, Taiwan.
[3]Department of Earth Sciences, National Cheng Kung University, Tainan, Taiwan.
[4]Observatoire Océanologique de Villefranche, Géosciences Azur, Villefranche-sur-Mer, France.
[5]Institute of Earth Sciences, Academia Sinica, Taipei, Taiwan.

0148-0227/10/2009JB006417

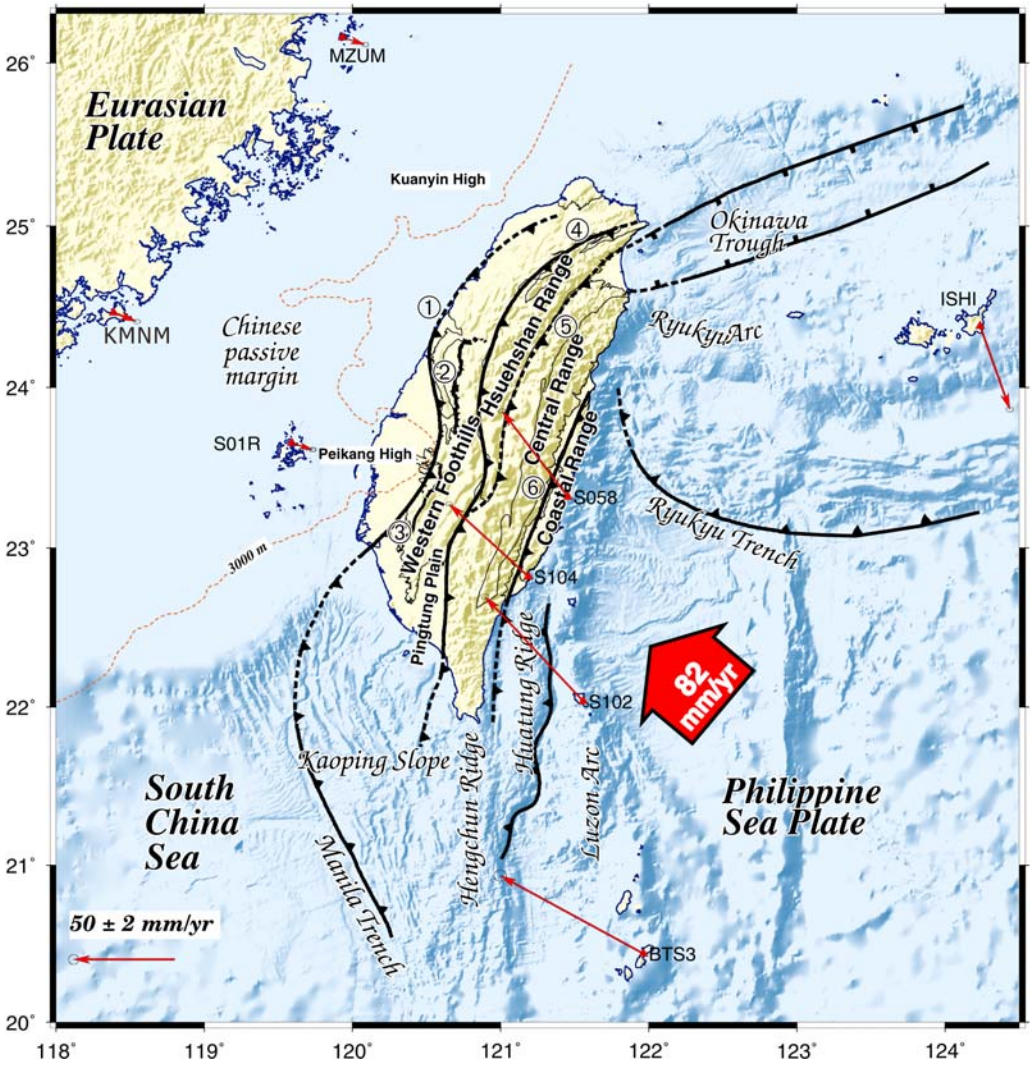

Figure 1. Relief map and geodynamic framework of the Taiwan region. Subduction along the Ryukyu and Manila trenches is shown as a solid line with triangles on the overriding plate. The large red indicator arrow notes direction and convergence rate between the volcanic arc and continental margin. The enumerated major structures (1–6) are the deformation front, the Chelungpu fault, the Chuchih fault, the Lishan fault, and the Longitudinal Valley fault. GPS velocity vectors are displayed as thin red arrows respect to stable Eurasia, following *Yu et al.* [1999].

mation [*Dixon*, 1991; *Segall and Davis*, 1997; *Thatcher*, 2003]. In Taiwan, the first island-wide "Taiwan GPS Network" was established in 1989. This network is composed of more than 150 epoch-surveyed stations and nine continuously recording stations covering the entire island of Taiwan and several offshore islets and annually surveyed since 1990. The results of satellite positioning (GPS) analyses from 1990 to 1995 (Figure 2) primarily revealed the interseismic velocity field within the seismogenic portion of the lithosphere [*Yu et al.*, 1997, 1999; *Hsu et al.*, 2003; *Johnson and Segall*, 2005; *Hsu et al.*, 2009a] (Figure 3).

[4] After the 1999 Chi-Chi earthquake, large coseismic deformation was mainly surveyed by campaign mode GPS measurements [*Yang et al.*, 2000; *Yu et al.*, 2001; *Hsu et al.*, 2007]. From 1993 to 2000, the Central Weather Bureau set up 17 continuous GPS stations in Taiwan [*Lin et al.*, 2006]. Severe limitations in the interpretation of continuous GPS data as representative of the permanent deformation were highlighted by the coseismic deformation of the destructive 1999 Chi-Chi earthquake (M_w = 7.6), which produced an ~100 km surface rupture in central west Taiwan.

[5] After this major earthquake, several institutions established continuous GPS stations for the assessment of potential seismic hazards in Taiwan. To investigate the postseismic activity following the Chi-Chi earthquake and the crustal deformation, the Seismological Observation Center of the Central Weather Bureau cooperated with the Institute of Earth Sciences, Academia Sinica to establish the Continuous Global Positioning System Network in Taiwan (TCGN). In the 15 month period following the earthquake,

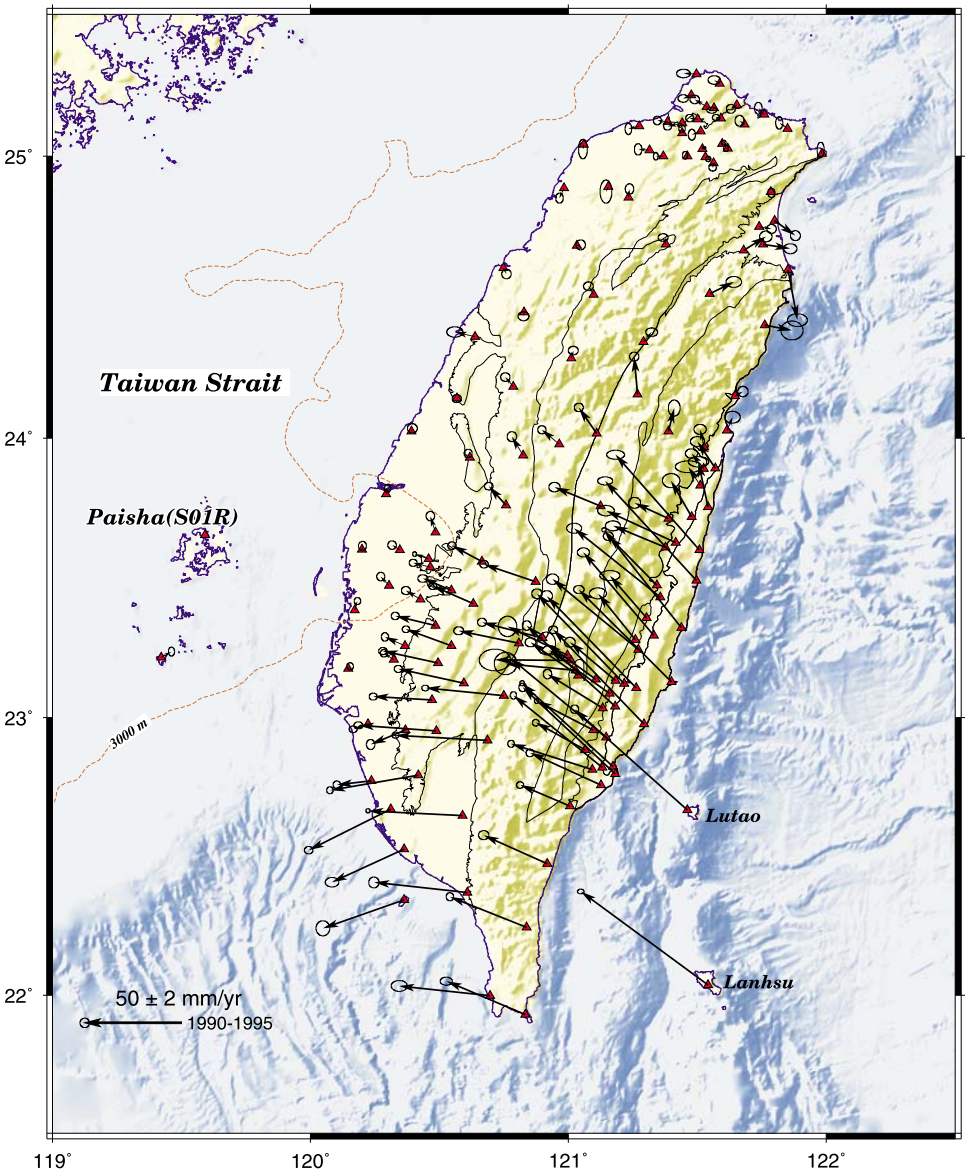

Figure 2. Results of the Taiwan GPS Network surveyed four to six times from 1990 to 1995 with dual-frequency geodetic receivers (as modified from GPS data of Table 2 of *Yu et al.* [1997]). Displacement is relative to the Paisha station, S01R, located in Penghu Island in the Chinese continental margin. The velocity vectors of stations in Lanhsu, Lutao, and the Coastal Range trend toward azimuths of 306°–322°, with rates of 56–82 mm/yr. The 95% confidence error ellipse is shown at the tip of each velocity.

the GPS stations of the hanging wall displayed significant postseismic deformation with a horizontal displacement of up to 252 mm toward the WNW and an uplift of 229 mm [*Yu et al.*, 2003; *Hsu et al.*, 2002].

[6] In previous studies, northern Taiwan is characterized as a transition zone because of compression due to plate convergence to transtension influenced by the Ryukyu subduction system [*Hu et al.*, 1996, 2001, 2002; *Rau et al.*, 2008], enhanced by extrusion and lateral escape toward the northeast [*Angelier et al.*, 2009]. These southeastward increasing station velocities are interpreted as a consequence of lateral extrusion due to the oblique collision between the Philippine Sea plate and the Eurasian plate [*Angelier et al.*, 2009], compatible with the back-arc opening of Okinawa trough [*Hou et al.*, 2009].

[7] From the structural point of view, the fold-and-thrust belt in west central Taiwan includes major trending thrust sheets [*Ho*, 1986] separated by some transfer faults [*Deffontaines et al.*, 1997]. Major seismicity occurred in the upper crust above a major décollement at a depth of ~10 km [*Carena et al.*, 2002]. The coseismic and postseismic deformation of Chi-Chi earthquake was analyzed from GPS and interferometric synthetic aperture radar (InSAR) data [*Yu et al.*, 2001, 2003; *Pathier et al.*, 2003; *Johnson and Segall*, 2004; *Savage et al.*, 2005; *Hsu et al.*, 2007].

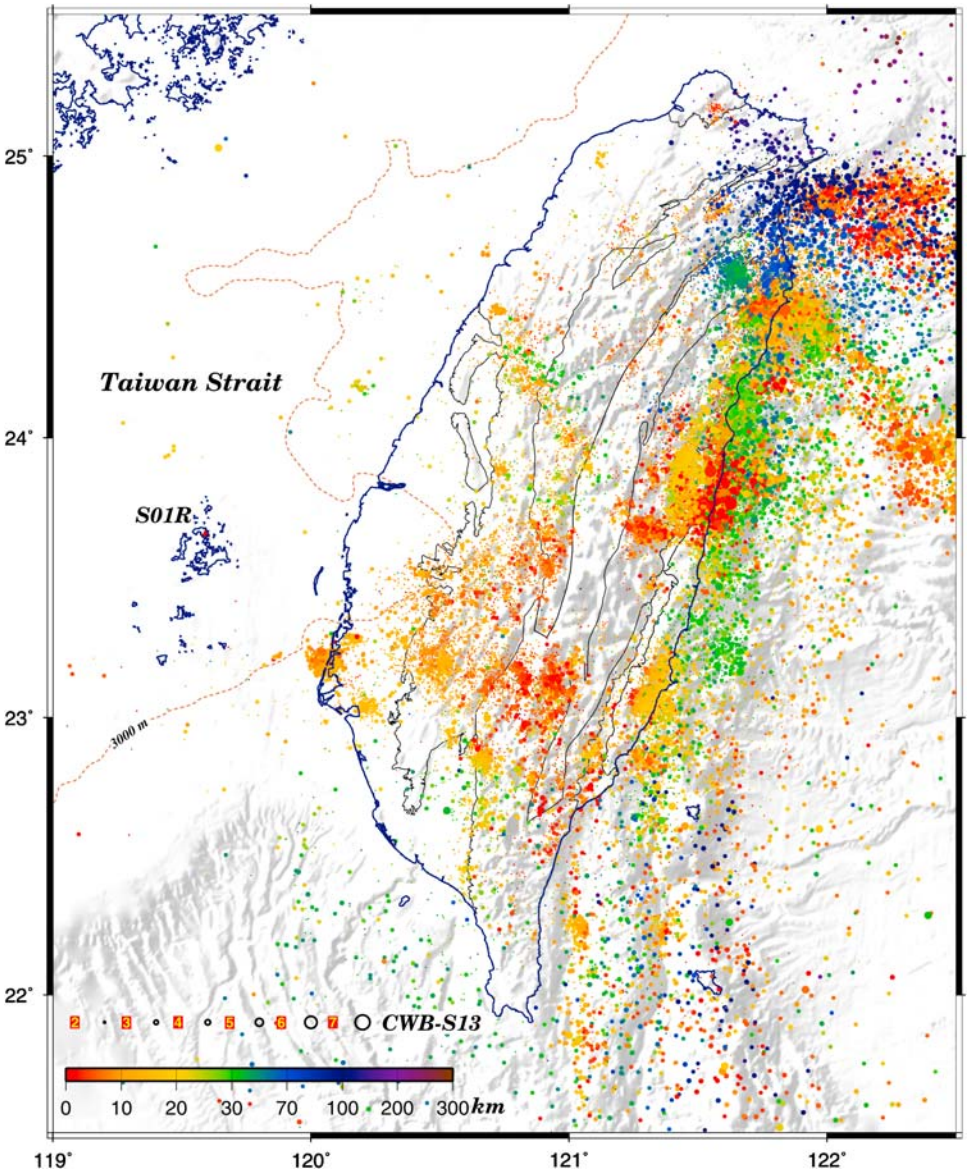

Figure 3. The earthquake distribution in Taiwan from 1990 to 1995. Dots indicate epicenter locations taken from the CWB network records with size increasing with magnitude and color depending on depth (see the scale bar).

[8] Southern Taiwan is located in the transition zone between subduction to the south and collision to the north [*Hu et al.*, 1997, 2001, 2006]. Lateral escape and extrusion occur toward the southwest, and the corresponding velocity field shows a counterclockwise movement, the rotation being nonrigid [*Lacombe et al.*, 2001; *Angelier et al.*, 2009]. According to this velocity pattern, southwestern Taiwan can be divided into three main domains separated by the Chukou fault and the Chishan fault [*Ching et al.*, 2007].

[9] The pattern of relative displacement in eastern Taiwan is dominated by the presence of an active plate suture, the 100–150 km long Longitudinal Valley Fault (LVF) zone where about one third of the total NW–SE convergence occurs with high seismicity [*Yu and Kuo*, 2001]. LANY in Lanhsu Island a value significantly larger than the previous report of permanent station S102, giving a velocity of 81.5 ± 1.3 mm/yr with directions of 306° ± 1° [*Yu et al.*, 1997].

[10] The most significant shortening occurred across the Chihshang Fault [*Angelier et al.*, 1997, 2000; *Lee et al.*, 2003, 2006], with a shortening rate of ~67 mm/yr. During our survey, the M_w = 6.8 Chengkung earthquake occurred on 10 December 2003, rupturing the Chihshang Fault. The footwall moved toward the north or NNE to the north, the east or ESE in the central area, and the SW or SSW to the south. The maximum horizontal coseismic displacement was about 4.5 cm (at station S055). Concerning the hanging wall in the Coastal Range, the coseismic displacements revealed a clear fan-shape with north or NNE trends to the

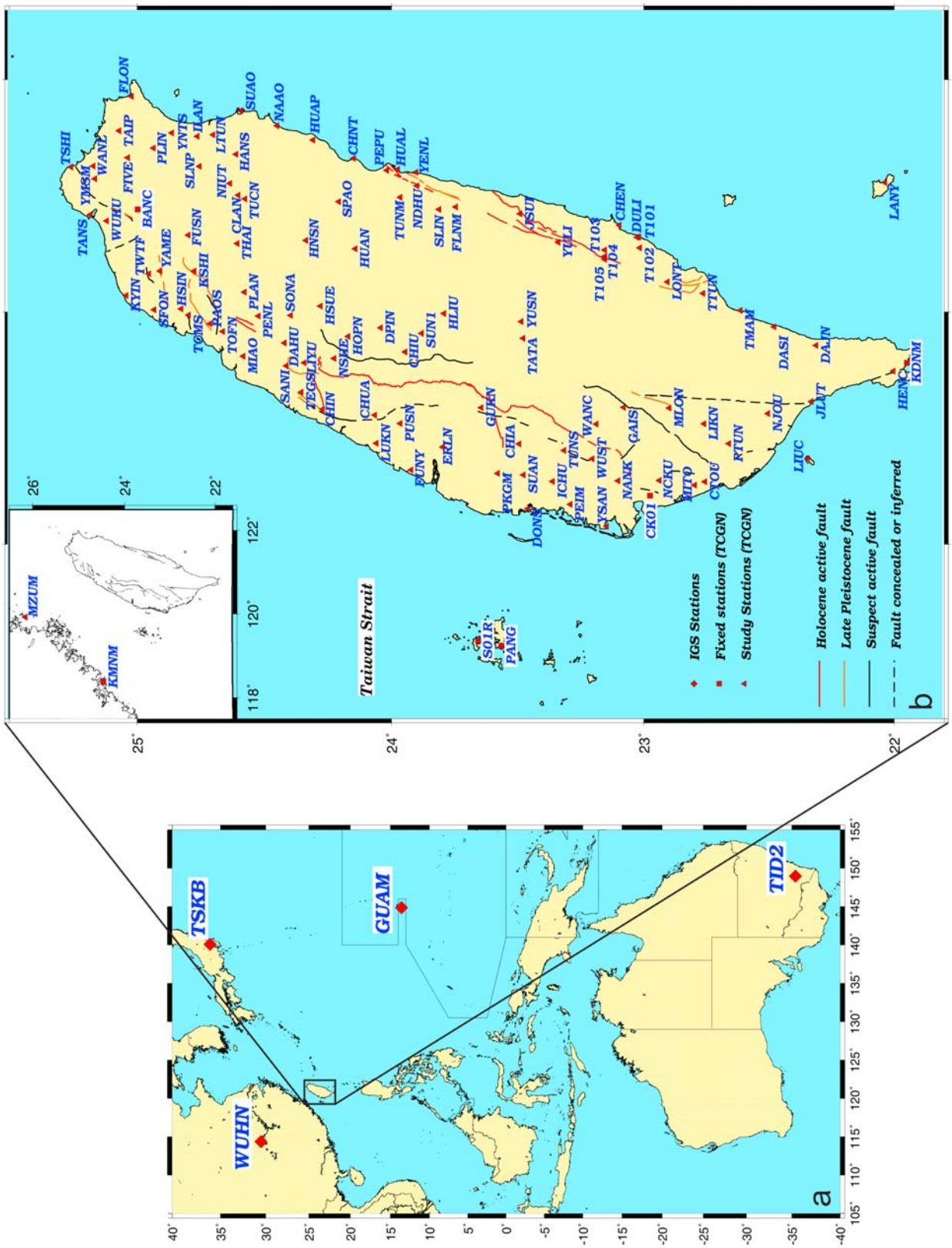
a
b
TSKB
GUAM
TID2
WUHN
Taiwan Strait
IGS Stations
Fixed stations (TCGN)
Study Stations (TCGN)
Holocene active fault
Late Pleistocene fault
Suspect active fault
Fault concealed or inferred

Figure 4

Table 1. Velocity Field in Six Fix Stations of TCGS[a]

Station	x (m)	y (m)	z (m)	V_x (m/yr)	V_y (m/yr)	V_z (m/yr)
PANG	−2886040.4700	5087844.0508	2534228.1617	−0.0325	−0.0112	−0.0152
S01R	−2886619.4687	5082945.0487	2543377.5267	−0.0316	−0.0111	−0.0134
KDNM	−3028999.6639	5084820.6278	2369241.3961	0.0118	0.0122	−0.0038
BANC	−3017225.6390	4934850.1827	2678851.6069	−0.0311	−0.0155	−0.0106
KMNM	−2761837.4487	5110347.2901	2625151.1085	−0.0328	−0.0121	−0.0145
CK01	−2956266.0799	5077239.8373	2474278.4333	−0.0199	−0.0039	−0.0144

[a]The x, y, z and V_x, V_y, V_z are the coordinates and average velocities in the Earth-Centered, Earth-Fixed Coordinate System, respectively.

north, NW or west trends in the middle area, and SW trends to the south. The coseismic displacement of the Chengkung earthquake reached ~126 mm in the horizontal component and 263 mm in the vertical component [*Chen et al.*, 2006; *Hu et al.*, 2007; *Hsu et al.*, 2009b], and the postseismic displacement in 109 days approached 59 and 68 mm, respectively, in the same components [*Chen et al.*, 2006; *Cheng et al.*, 2009; *Hsu et al.*, 2009b]. The maximum horizontal and vertical coseismic displacements near the epicentral area reached about 12.6 and 26.3 cm, respectively, at station S033 [*Chen et al.*, 2006; *Ching et al.*, 2007; *Hu et al.*, 2007]. Near the epicentral area, velocities at several stations were affected by the coseismic and postseismic deformation of the Chengkung earthquake by up to ~10 mm/yr.

[11] As a main aim of this paper, it is thus crucial to determine whether the GPS velocity field reveals steady state deformation or simply reflects the interseismic stage of variable deformation during the earthquake cycle. On the basis of continuous GPS data, we discuss the seismic deformation for large events during the period 2003–2005, taking advantage of its daily time series. We thus examine and compare displacement and strain patterns (relative strain magnitudes, dilatational strain and rotational strain components) before and after the large 1999 Chi-Chi earthquake and before and after three other relatively large earthquakes. We quantify in more detail than previous campaign mode results [*Yu et al.*, 1997] both the velocity distribution and the strain rate field to better characterize the style of present-day deformation along a convergent plate boundary. We also compare the velocities before and after Chi-Chi earthquake in order to better characterize the influence of the earthquake cycle.

2. Data Acquisition and Processing

2.1. Continuous GPS Network

[12] Completed in 2005, the TCGN incorporated 200 continuous GPS stations with a multifunction monitoring system and variable station spacing depending on seismotectonic activity and population density of <20 km on average. The TCGN receivers have a high sampling rate, safe data storing devices, and a facility for real-time transmission equipment. The short-term priority involves detection of preseismic, coseismic, and postseismic movements related to large events. The long-term mission of the TCGN is to monitor the crustal deformation related to plate convergence. For this study, we collected daily continuous GPS data from 1 January 2003 to 31 December 2005 at 114 sites (Figure 4), including 96 stations from the Central Weather Bureau (CWB), 7 stations from the Ministry of the Interior, 5 stations from National Taiwan University, 2 stations from National Cheng Kung University (NCKU), and 4 International Global Navigation Satellite Systems Service (IGS) sites (WUHN, GUAM, TSKB, and TID2).

2.2. GPS Data Processing

[13] In each survey, all stations are observed simultaneously with dual-frequency geodetic receivers. The antenna types include ROUGE SNR-8000, AOAD/M_T, Leica RS500, LEIAT504 SCIS, TRIMBLE 5700, and TRM41249.00, or their equivalents. Most sites are equipped with choke ring antenna with radome. The sampling interval for data collection is 30 s. The raw data of each station are transferred to the Receiver-Independent Exchange Format (RINEX) format. The continuous GPS data were processed session by session with the Bernese software version 4.2 [*Hugentobler et al.*, 2001] in two steps to obtain precise coordinates.

[14] During the preprocessing step, the data were checked and prepared for coordinate estimation. Satellite orbits were converted into the Bernese format first, and a standard arc orbit for each day was generated, then the RINEX data files were translated into Bernese format. We analyzed P code to evaluate the receiver-clock errors on the microsecond level and estimated station coordinates using zero difference code measurements. The baselines were accumulated from simultaneous phase and code single-difference observations between receivers. The triple-difference algorithm was used for detecting cycle slips for all observations.

[15] During the postprocessing step, double-difference observations were used to determine station coordinates. We used the ephemerides provided by IGS. Using ionosphere-free linear combination of carrier phase observations at L_1 and L_2 frequencies, L_3, the first-order ionospheric effects were removed. The data obtained from elevation cutoff

Figure 4. (a) Four global IGS fiducial stations surrounding Taiwan (TSKB, GUAM, TID2, and WUHN) on the international terrestrial reference frame (ITRF2000) are used to determine the positions and velocities of six local GPS continuous-recording stations (BANC, CK01, KDNM, KMNM, S01R, and PANG) from 1994 to 2005 by minimizing common-mode deviations from linear velocities. (b) TCGN stations used in this study. The fault traces are from *Lin et al.* [2000].

angle lower than 15° were not used to reduce multipath effects and noise. Tropospheric refraction corrections were based on the atmospheric zenith delay model [*Saastamoinen*, 1973]. The difference between actual and calculated zenith delays, or residual tropospheric zenith delay, was estimated every 2 h per station in the least squares adjustment of carrier phase observations [*Brunner and Welsch*, 1993].

[16] Four global IGS fiducial stations (TSKB, GUAM, TID2, and WUHN) (Figure 4a) in the international terrestrial reference frame ITRF2000 [*Altamimi et al.*, 2002] were used to determine the positions and velocities of six local permanent stations (BANC, CK01, KDNM, KMNM, PANG, and S01R) by minimizing common mode deviations from linear velocities [*Tabei and Amin*, 2002] (Table 1). Then the coordinates of 110 continuous GPS (CGPS) stations in Taiwan (Figure 4b) were calculated from the positions of six local stations with coordinates derived from a priori positions and velocities. Following previous authors [*Yu et al.*, 1997], we chose the Paisha station, S01R, as the reference for the velocity field. This choice is convenient because this station belongs to the South China Block, the stable foreland of the Taiwan mountain belt.

2.3. Improved Time Series

[17] The analysis included the following steps. First, the GPS time series were defined for each component using the least squares method as modified from *Nikolaidis* [2002]. according to

$$y(t_i) = a + bt_i + \sum_{j=1}^{n_c} c_j H(t_i - T_{cj}) + \sum_{j=1}^{n_d} d_j H(t_i - T_{dj}) t_i + \sum_{j=1}^{n_e} e_j \log(t_i - T_{ej}) H(t_i - T_{dj}) + v_i, \quad (1)$$

where t_i for $i = 1, N$ are the daily solution epochs in units of years, and H is the Heaviside step function. The first two terms involve the site position, *a,* and the linear rate, *b*. The third term corrects for any number (n_c) of offsets with magnitudes **c** and epochs T_c. The postseismic motion is introduced as a rate change, d_j, and a logarithmic decay with magnitude, e_j, at the selected earthquake epochs T_{dj} and T_{ej}. The measurement error is v_i. We then applied the spatial filtering technique to remove common mode errors from coordinate time series. The method proposed by *Wdowinski et al.* [1997] includes detrending, stacking, and filtering.

2.4. Determination of Strain Rate From CGPS Data

[18] In contrast to the displacement data, the strain rate tensor is independent of the reference frame. The strain rate field reveals local strain accumulation rates and their possible connection to seismic hazard potential [*Ward*, 1994]. We derived strain rates from the velocity estimates according to the procedure described by *Shen et al.* [1996]. This method, following previous methods [e.g., *Frank*, 1966; *Prescott*, 1976], interpolates the strain rates from local geodetic measurements through continuous functions within the entire network.

[19] At each location, a uniform strain rate field is assumed, and a least squares inversion is performed over strain velocity solutions and their covariance for six unknowns. As shown in Figure 9, we thus estimated the strain rate distribution according to that of the GPS velocity gradients based on

$$\begin{bmatrix} v_e^i \\ v_n^i \end{bmatrix} = \begin{bmatrix} 1 & 0 & \Delta x_{ij} & \Delta y_{ij} & 0 & \Delta y_{ij} \\ 0 & 1 & 0 & \Delta x_{ij} & \Delta y_{ij} & -\Delta x_{ij} \end{bmatrix} \begin{bmatrix} v_e^j \\ v_n^j \\ \dot{\varepsilon}_{ee}^j \\ \dot{\varepsilon}_{en}^j \\ \dot{\varepsilon}_{nn}^j \\ \dot{\omega}^j \end{bmatrix} + \begin{bmatrix} e_e^i \\ e_n^i \end{bmatrix}, \quad (2)$$

where the horizontal velocity components (v_e^j, v_n^j), the strain rate components ($\dot{\varepsilon}_{ee}^j$, $\dot{\varepsilon}_{en}^j$, $\dot{\varepsilon}_{nn}^j$), and a rotation rate $\dot{\omega}^j$ at a particular point j (x_j, y_j) are related with the observed velocity components (v_e^i, v_n^i) at an observation point i (x_i, y_i), while $\Delta x_{ij} = x_i - x_j$ and $\Delta y_{ij} = y_i - y_j$ (e_e^i, e_n^i) are the observational errors.

3. Changes in Deformation Patterns Related to Major Earthquakes

3.1. Major Earthquakes in Taiwan, 2003–2005

[20] On the basis of the catalog of the Broadband Arrays in Taiwan for Seismology, 22 earthquakes with magnitudes $M_w \geq 5$ occurred around Taiwan, 6 of them being located within Taiwan inland during our survey period (Figure 5). Four large events occurred in eastern Taiwan and resulted in significant coseismic and postseismic deformation or peculiar swarm pattern. The first is the 10 December 2003 M_w = 6.8 Chengkung earthquake. On 5 March 2005, two earthquakes about the same magnitude, M_w = 5.9, occurred within 68 s called the Ilan double earthquakes. North of Hualien, an earthquake swarm developed from 1 January to 4 April in 2005. Then a second swarm of earthquakes occurred in Hualien city from 5 to 17 April. After that, the third swarm of earthquakes occurred in the northern and southern part in the same area as before. On 30 April 2005 the largest earthquake, about M_w = 5.6 (Hualien earthquake), occurred in Hualien city. For the sake of simplicity, we designated these earthquakes as event 1 (2003 Chengkung earthquake), event 2 (2005 Ilan doublet), event 3 (2005 Ilan doublet), and event 4 (2005 Hualien earthquake). Events 1 and 4 occurred at the active tectonic boundary in Taiwan where the last major events had been the Hualien-Yuli-Taitung earthquakes of 1951.

3.2. CGPS Time Series and Velocities

[21] To investigate the secular velocity field in the period of 2003–2005, we chose six CGPS stations in the epicentral area of the four events to better characterize the influence of the coseismic and postseismic deformation associated with these events (Figure 6). At station CHEN, a nearly 1 year period before event 1 indicates displacement with a constant velocity (43 and 55 mm/yr for the north and west compo-

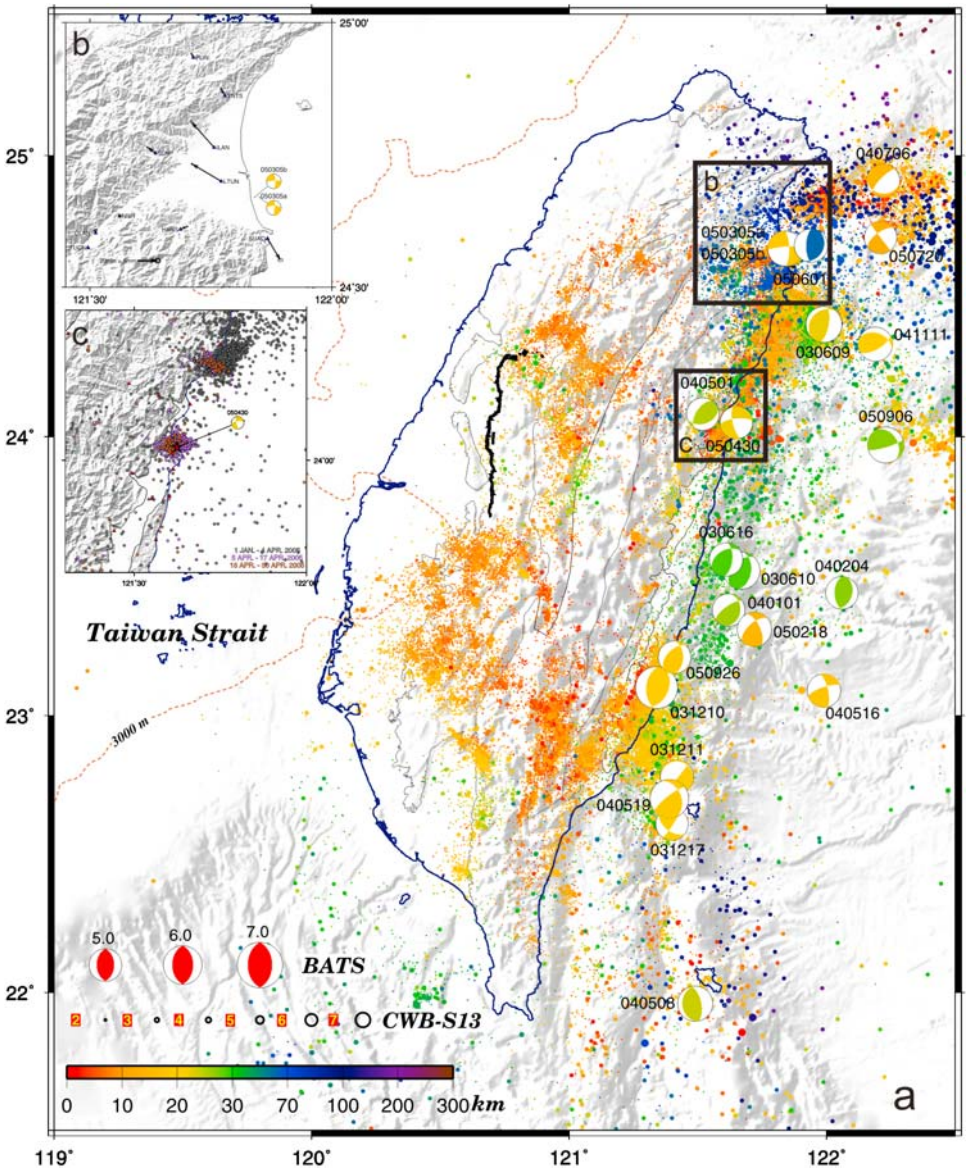

Figure 5. (a) Events recorded by the CWB network and focal mechanisms of 22 earthquakes with magnitudes $M_w \geqq 5$ from the BATS network, for the period 2003–2005. The main shock related to the 10 December 2003 $M_w = 6.8$ Chengkung earthquake is referenced as 031210. (b) The coseismic displacement of the 5 March 2005 $M_w = 5.9$ Ilan double earthquakes (050305a and 050305b). (c) The earthquake clusters occurring before 30 April 2005 $M_w = 5.6$ the Hualien earthquake (050430) in eastern Taiwan, discussed in this paper.

nents, respectively; that is, 70 mm/yr in the N52°W direction). Then the earthquake, as the largest one of the analyzed period in Taiwan, induced major displacement toward the northeast (95 and 86 mm for the north and east components, respectively; that is, 128 mm in the N42°E direction).

[22] This coseismic displacement was followed by relatively fast postseismic displacement during the 3 months following the earthquake, resulting in additional displacement of ~35 mm (33 and 12 mm for the north and east components, respectively), with a progressive clockwise rotation of the displacement vector illustrated in Figure 6 by the curved distribution of data points for these 3 months following event 1. Later in 2004 and 2005, the displacement became constant in velocity as before the earthquake (with 54 and 49 mm/yr for the north and west components, respectively; that is, 91 mm/yr in a N42°W direction).

[23] The interseismic and coseismic displacements occurred in nearly perpendicular directions (N52°–42°W and N42°E, respectively), and the velocity was significantly larger after the event 1 than before (91 mm/yr instead of 70 mm/yr). Figure 6 also shows that the slow subsidence of station CHEN in 2003 (~11 mm/yr) was interrupted by a strong coseismic uplift of ~150 mm during the Chengkung earthquake and >30 mm over the following 3 months. During the next 22 months, uplift occurred at a rather stable rate of 28 mm/yr.

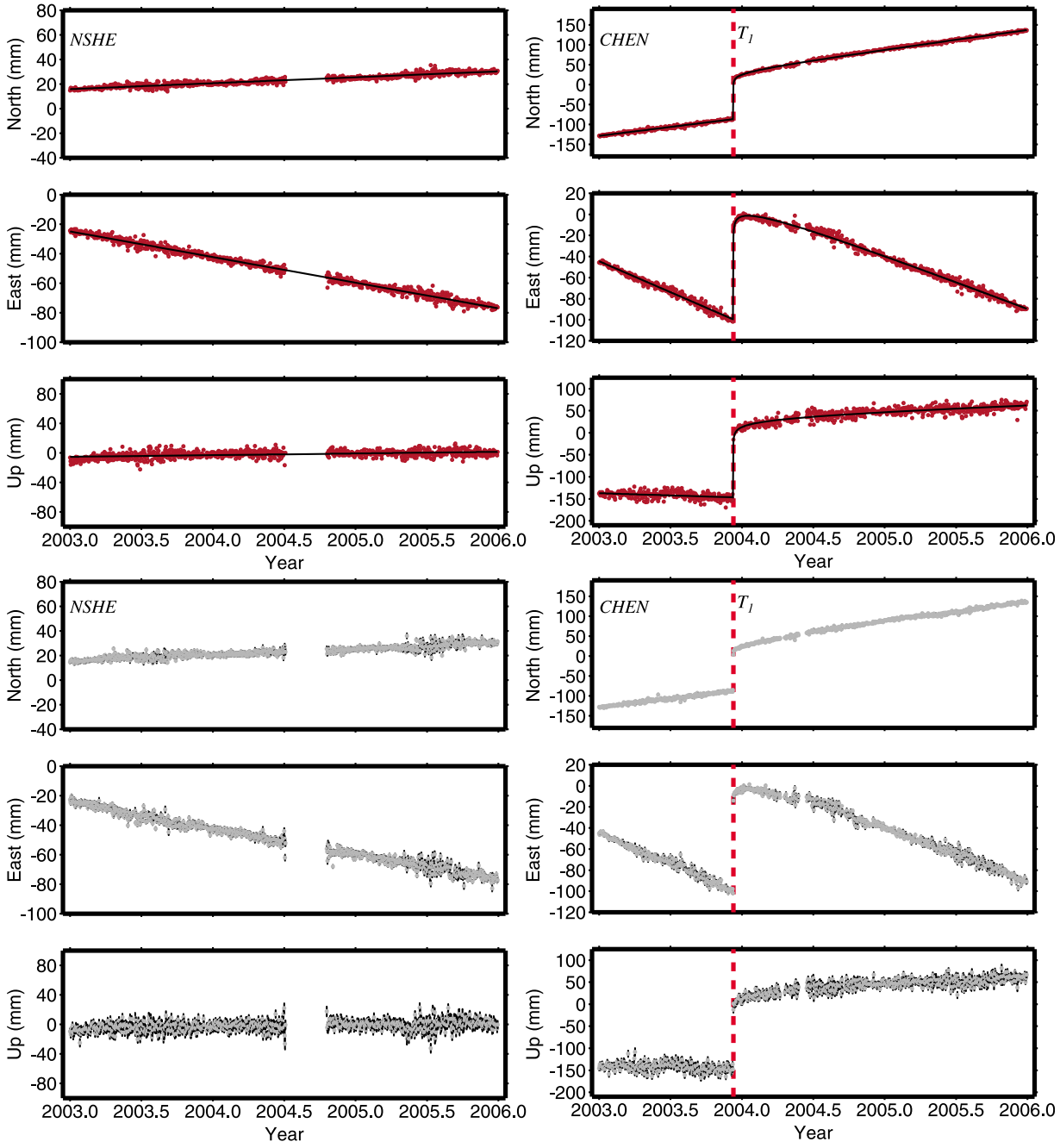

Figure 6. Time series of coordinate changes relative to the stable continental margin, Paisha, Penghu (S01R), in the north, east, and up components. Identical displacement scales in mm (ordinates) and time scales in years (abscissas). (top) The filtered time series and (bottom) the prefiltered time series. Continuous displacement data were recorded from 1 January 2003 to 31 December 2005. The red dashed lines (T_1, T_2, T_3, and T_4) refer to the Chengkung earthquake, Ilan double earthquakes, and the Hualien earthquake (references 031210, 050305a, 050305b, and 050430), respectively, in Figure 5.

[24] Station CHEN is located at a short distance from the epicenter of the Chengkung earthquake in the hanging wall of the reverse Chihshang Fault activated during this earthquake. Station TUNS is located in the footwall, on the opposite side of the mountain belt, at a distance of ~110 km from the epicenter. At this station, the displacement related to event 1 and its aftershock sequence is ~5 mm to the south and 10 mm to the east (that is, 11 mm in a N117°E direction), with a subsidence of nearly 10 mm (Figure 6). In contrast with station TUNS, station NSHE, located at a similar across-belt distance but at a large along-belt distance to the north, did not reveal significant displacement during event 1.

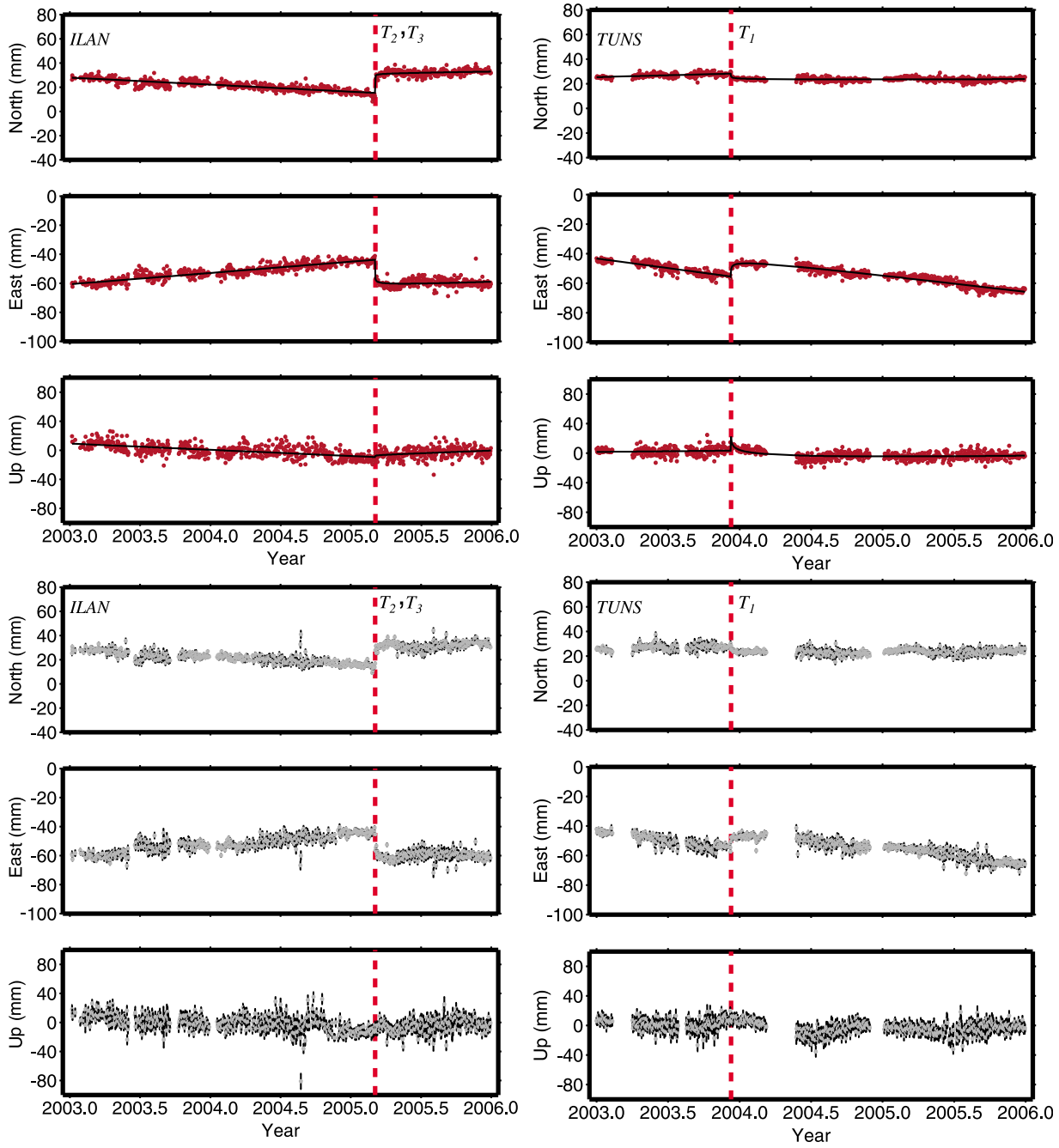

Figure 6. (continued)

[25] The other major earthquakes of our study period affected displacement at stations ILAN for the events 2 and 3 and YENL for event 4. In the first case, the coseismic displacement is about 26.5 and 23.5 mm for the north and west components, indicating ~35.4 mm of displacement toward the northwest, consistent with the strike-slip mechanism of the earthquake (Figure 5 and Table 2). The case of event 4 recorded in station YENL differs, in that no significant difference exists between the average displacement velocity vectors before and after the earthquake. However, the coseismic displacement to the southeast during event 4 is also consistent with the strike-slip mechanism (Figure 5) and the position of station YENL (Figure 4). The time series of all stations are listed in the auxiliary material.[1]

[26] With respect to Paisha station, S01R, the stations are moving toward the northwest at 20 mm/yr (PENL) to 4–5 mm/yr (PAOS and TCMS) in the Miaoli-Hsinchu area. The velocities decrease northward with a marginally insignificant station in Taipei area. Larger velocities affect the Ilan area: 9.7 and 17.2 mm/yr with directions of 126° and 128°, respectively, for stations ILAN and LTUN in central Ilan

[1] Auxillary materials are available in the HTML. doi:10.1029/2009JB006417.

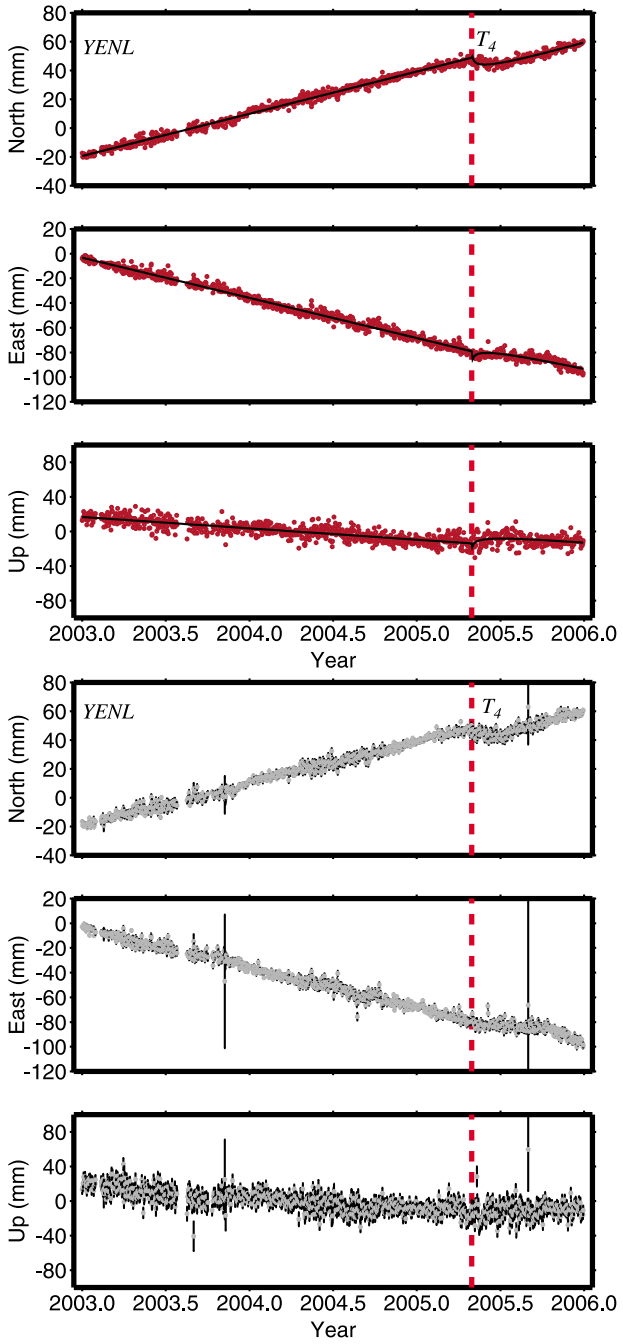

Figure 6. (continued)

Plain, up to 32.8 mm/yr with direction of 146° for station SUAO farther south. In western Taiwan, the velocities in the inner fold-and-thrust belt range from 14.2 to 45.5 mm/yr with directions of 284°–304°. They decrease to values <10 mm/yr in the outer fold-and-thrust belt and the Coastal Plain, consistent with strain accumulation across the fold-and-thrust belt.

[27] The velocities are small in the rim of Peikang basement high area (stations CHIA and TUNS, 11.7 and 12.8 mm/yr, respectively) and increase to the south with significant counterclockwise deviation. Stations MLON, LIKN, and PTUN in the Pingtung Plain revealed velocities ranging from 48.7 to 55.4 mm/yr with directions of 262°–308°, consistent with a right-lateral component along the Chishan reverse fault. Velocities for stations on the Coastal Range to Lanhsu are 40.5–93.6 mm/yr with directions of 307°–333°. The maximum station velocity is 93.6 mm/yr with direction of 307° (LANY on Lanhsu Island). The minimum station velocity is 40.5 mm/yr with direction of 310° at YENL in the north segment of the coastal range. The stations in the western side of the coastal range (the Longitudinal Valley and Central Range) revealed velocities in the range 19.0–49.3 mm/yr with directions of 285°–318°. A discontinuity in station velocity of ~10 mm/yr is absorbed between stations YENL and TUNM across the two branch fault of the northern LVF, and a similar discontinuity occurs across the horsetail structures at the northern tip of the Longitudinal Valley (between stations HUAL and PEPU) (Figure 7 and Table 3).

3.3. Spatial Variation of Crustal Strain Rates in Taiwan

[28] The changes in baseline lengths from the repeated and CGPS surveys were used to assess the spatial variation of the horizontal crustal strain over the region. On the basis of the distribution of geodetic stations (Figure 4) and systematic interpolation, the strain rate field could be calculated in a regular grid, as shown in Figure 9. Two assumptions were made: uniform spatial accumulation of crustal strain within each mesh and constant rate of strain accumulation over each time period considered. The analyses of changes in baseline length based on the 2003–2005 CGPS data (Figure 6) provide detail and allow validation of the second hypothesis. The strain rates are given in units of microstrain per year (1 μstrain = 10^{-6}). Positive values denote extension, while negative values represent shortening or contraction.

[29] Negative values prevail in the Coastal Range and the foothills, where active thrusting is clearly documented (Figure 8). Positive values of strain rate are present at both tips of the collision belt where extrusion occurs and also along the High Central Range, where normal faulting is indicated by both the geological observation and the focal mechanisms of earthquakes.

[30] Extensional strain rates occur in the Ilan Plain and Pingtung Plain areas at the tips of the collision belt (light blue and dark blue domains in Figure 8). The largest extensional rate of our survey period (Figure 8b) was found in the Ilan Plain, with 2.66 μstrain/yr in a NW–SE direction and a shortening rate of 1.28 μstrain/yr in a NE–SW direction (azimuths 132°–150°), which revealed transtension. Because this area is considered as a western extension of the Okinawa trough [*Liu*, 1995], the extensional deformation is assumed to be related to extension in the Okinawa trough [*Letouzey and Kimura*, 1985; *Sibuet et al.*, 1987]. Transtension also occurs, with significant albeit smaller rates, in the Pingtung Plain area of southwest Taiwan. These deformations result from extrusion and lateral escape at both tips of the Taiwan collision belt [*Angelier et al.*, 2009].

3.4. Rotation Components

[31] In Figure 9, the periods distinguished are the same as in Figure 8. A significant clockwise rotation of up to 1.2–1.5 μrad/yr occurs near the southern part of the Ilan Plain, consistent with the conclusions of *Liu* [1995], who

Table 2. Horizontal and Vertical Coseismic Deformation of Ilan Double Earthquakes From Continuous GPS Measurements With Respect to Paisha Station in Penghu[a]

Stations	Longitude (deg)	Latitude (deg)	S_E (mm/yr)	S_N (mm/yr)	S_U (mm/yr)	Err_E (mm/yr)	Err_N (mm/yr)	Err_U (mm/yr)
CLAN	121.5120	24.6023	0.1	2.9	−0.1	0.56	0.46	1.54
HANS	121.6871	24.6095	7.1	2.9	−0.3	0.28	0.29	0.90
ILAN	121.7566	24.7640	−23.5	26.5	12.6	0.55	0.54	1.49
LTUN	121.7716	24.7000	−30.3	18.0	5.3	0.33	0.30	0.85
NIUT	121.5615	24.6347	−0.2	0.2	−5.2	0.30	0.30	1.01
PLIN	121.7139	24.9336	−2.1	4.1	−2.2	0.32	0.33	0.99
SLNP	121.6356	24.7531	−8.4	6.3	0.3	0.27	0.27	0.84
SUAO	121.867	24.5923	13.3	−22.5	−1.1	1.00	0.71	1.77
TUCN	121.4961	24.5748	0.6	−0.4	−13.2	0.30	0.28	1.34
YNTS	121.7789	24.8617	−4.0	7.3	9.2	0.41	0.42	1.14

[a] S_N, S_E, and S_U are north, east, vertical slip, respectively; Err_N, Err_E, and Err_U are errors, respectively.

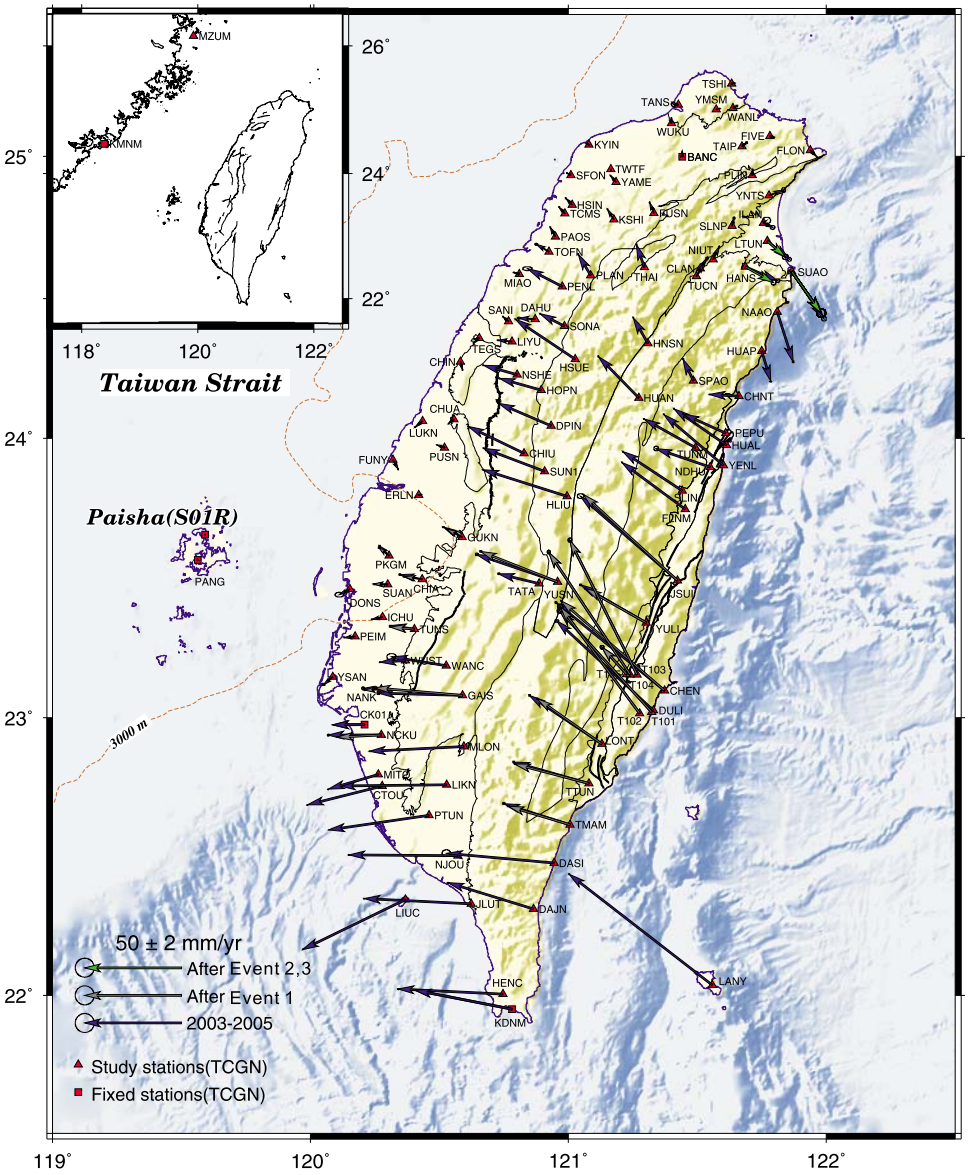

Figure 7. The 110 GPS stations from the TCGN used in our study. The GPS velocities field of Taiwan is with respect to station S01R. The blue arrows indicate the average velocities from 2003 to 2005. The gray arrows indicate the velocities after the Chengkung earthquake. The green arrows indicate the velocities after the Ilan double earthquakes.

Table 3. Velocities Field in 104 Stations[a]

Stations	Longitude (deg)	Latitude (deg)	V_E (mm/yr)	Err_E (mm/yr)	V_N (mm/yr)	Err_N (mm/yr)	V_U (mm/yr)	Err_U (mm/yr)	V (mm/yr)	Azimuth (deg)
CHEN	121.3736	23.0974	−56.2	0.2	45.5	0.2	−0.1	0.6	72.3	309
CHIA	120.4332	23.496	−11.4	0.2	2.4	0.2	1.1	0.5	11.7	282
CHIN	120.5822	24.271	1.0	0.1	−4.0	0.1	−8.7	0.1	4.2	166
CHIU	120.8289	23.9454	−28.9	0.1	14.0	0.1	4.2	0.1	32.1	296
CHNT	121.6619	24.1492	−15.2	0.1	0.9	0.1	−4.5	0.1	15.2	273
CHUA	120.5573	24.0661	−2.8	0.1	−2.1	0.1	−3.2	0.1	3.5	234
CLAN	121.512	24.6023	3.5	0.3	5.5	0.2	8.8	0.7	6.5	33
CTOU	120.2778	22.7547	−38.6	0.1	−9.7	0.1	1.2	0.2	39.8	256
DAHU	120.8718	24.4229	−8.3	0.4	0.5	0.2	−1.8	0.7	8.3	274
DAJN	120.865	22.3113	−44.1	0.2	13.6	0.1	−0.1	0.4	46.2	287
DASI	120.9444	22.4784	−55.6	0.9	5.0	0.7	62.1	2.9	55.9	275
DONS	120.1538	23.4605	−5.6	0.9	−2.8	0.5	5.8	2.6	6.2	243
DPIN	120.9328	24.0431	−27.1	0.1	11.6	0.1	8.4	0.1	29.5	293
DULI	121.3306	23.0257	−50.0	0.4	46.3	0.3	9.3	0.8	68.2	313
ERLN	120.4196	23.7976	1.4	0.1	0.1	0.1	−28.6	0.1	1.4	85
FIVE	121.7811	25.0711	2.2	0.1	−0.6	0.1	−2.2	0.1	2.3	105
FLNM	121.4534	23.7463	−32.8	0.1	24.2	0.1	−8.5	0.1	40.7	306
FLON	121.9375	25.0204	3.4	0.1	−3.4	0.1	−1.7	0.3	4.8	135
FUNY	120.3202	23.9223	2.7	0.1	−4.8	0.1	−48.0	0.1	5.6	151
FUSN	121.3315	24.799	−2.2	0.1	5.5	0.1	−2.2	0.1	5.9	338
GAIS	120.5906	23.0803	−43.6	0.3	1.2	0.3	15.0	1.4	43.6	272
GUKN	120.5888	23.6459	−9.7	0.2	5.3	0.1	−7.5	0.4	11.1	298
HANS	121.6871	24.6095	16.7	0.4	−7.2	0.4	−2.3	1.1	18.2	113
HENC	120.7465	22.0039	−54.1	0.1	2.6	0.1	−4.7	0.1	54.2	273
HLIU	120.9942	23.793	−43.4	0.1	13.7	0.1	10.0	0.2	45.5	288
HNSN	121.3081	24.3377	−7.5	0.1	13.2	0.1	8.7	0.1	15.2	330
HOPN	120.8949	24.1708	−21.6	0.1	6.1	0.1	5.0	0.4	22.4	286
HSIN	121.0143	24.8278	−3.3	0.1	3.5	0.1	−0.7	0.1	4.8	317
HSUE	121.0265	24.2806	−30.9	0.1	20.6	0.1	−13.9	0.2	37.1	304
HUAL	121.6135	23.9754	−27.2	0.1	18.8	0.1	1.6	0.6	33.1	305
HUAN	121.2726	24.1435	−20.9	0.1	21.4	0.1	2.5	0.1	29.9	316
HUAP	121.7494	24.309	4.7	0.2	−15.6	0.1	−4.0	0.4	16.3	163
ICHU	120.2793	23.3607	−5.4	0.1	−1.2	0.1	−0.4	0.2	5.5	258
ILAN	121.7566	24.764	4.7	0.5	−2.3	0.4	−1.3	1.2	5.2	116
JLUT	120.6228	22.33	−55.2	0.1	2.7	0.1	−2.7	0.3	55.3	273
JSUI	121.4239	23.492	−50.2	0.7	43.6	0.5	−9.4	1.8	66.5	311
KSHI	121.176	24.7767	−3.3	0.1	5.2	0.1	−1.1	0.1	6.2	328
KYIN	121.0804	25.0411	−1.4	0.1	0.7	0.1	−3.7	0.2	1.6	295
LANY	121.5581	22.0373	−74.0	0.1	57.3	0.1	1.2	0.2	93.6	308
LIKN	120.5279	22.7586	−55.4	0.1	−0.6	0.1	−4.0	0.2	55.4	269
LIUC	120.3691	22.3467	−53.1	0.1	−25.8	0.1	2.1	0.1	59.0	244
LIYU	120.7818	24.3431	−7.3	0.1	0.7	0.1	0.7	0.1	7.3	276
LONT	121.1306	22.9063	−37.4	0.2	25.1	0.2	6.8	0.6	45.1	304
LTUN	121.7716	24.7	11.4	0.4	−9.5	0.4	−0.5	1.2	14.8	130
LUKN	120.4351	24.06	−3.9	0.1	−3.1	0.1	−4.1	0.1	5.0	231
MIAO	120.8103	24.5835	−2.8	0.1	0.8	0.1	−3.1	0.1	2.9	285
MITO	120.2632	22.7959	−25.9	0.1	−7.6	0.1	5.2	0.3	27.0	254
MLON	120.5958	22.8967	−48.7	0.1	−2.5	0.1	2.8	0.4	48.8	267
MZUM	119.9332	26.1571	−1.4	0.1	0.3	0.1	−3.1	0.1	1.4	284
NAAO	121.8102	24.4493	8.3	0.2	−25.9	0.2	−6.1	0.5	27.2	162
NANK	120.2744	23.102	−9.3	0.3	0.5	0.3	−6.3	0.9	9.3	273
NCKU	120.2758	22.9385	−27.5	0.2	−0.1	0.2	−0.6	0.6	27.5	270
NDHU	121.5508	23.8972	−28.0	0.5	9.5	0.5	0.8	1.2	29.6	289
NIUT	121.5616	24.6348	3.1	0.1	6.7	0.1	−1.1	0.4	7.3	25
NJOU	120.5714	22.5039	−56.3	0.1	0.4	0.1	2.5	0.3	56.3	270
NSHE	120.8009	24.2258	−17.4	0.1	4.8	0.1	2.3	0.1	18.1	286
PAOS	120.9503	24.7149	−2.7	0.1	4.9	0.1	−0.4	0.1	5.6	331
PEIM	120.1728	23.2922	−5.4	0.1	−0.6	0.1	0.6	0.5	5.5	263
PENL	120.976	24.5388	−18.0	1.0	9.3	0.4	8.0	1.8	20.2	297
PEPU	121.6103	24.0179	−22.0	0.1	9.9	0.1	−2.4	0.1	24.1	294
PKGM	120.3055	23.5799	−5.0	0.2	5.0	0.2	−19.1	0.6	7.1	315
PLAN	121.0866	24.579	−6.4	0.1	10.9	0.1	−0.1	0.1	12.6	330
PLIN	121.714	24.9336	0.2	0.1	2.9	0.1	−4.5	0.2	2.9	3
PTUN	120.4597	22.6499	−51.9	0.1	−7.6	0.0	−0.4	0.2	52.5	262
PUSN	120.5201	23.9649	−0.2	0.1	0.3	0.1	−16.3	0.5	0.4	332
SANI	120.7687	24.4144	−3.0	0.1	2.5	0.1	−9.6	0.2	3.9	310
SFON	121.0102	24.9329	−2.0	0.1	1.1	0.1	−2.2	0.1	2.3	299
SLIN	121.4414	23.8119	−30.7	0.1	20.3	0.1	−3.9	0.1	36.8	303
SLNP	121.6356	24.7531	0.9	0.2	4.1	0.2	−1.3	0.7	4.2	13
SONA	120.9858	24.3978	−12.6	0.1	6.4	0.1	−0.5	0.2	14.2	297
SPAO	121.4849	24.205	−5.4	0.2	11.2	0.1	12.5	0.5	12.4	334

Table 3. (continued)

Stations	Longitude (deg)	Latitude (deg)	V_E (mm/yr)	Err_E (mm/yr)	V_N (mm/yr)	Err_N (mm/yr)	V_U (mm/yr)	Err_U (mm/yr)	V (mm/yr)	Azimuth (deg)
SUAN	120.2999	23.4776	−6.9	0.1	0.1	0.1	3.9	0.6	6.9	270
SUAO	121.8671	24.5924	16.6	0.5	−24.4	0.5	−0.7	1.7	29.5	146
SUN1	120.9084	23.8812	−31.6	0.1	12.0	0.1	7.9	0.1	33.8	291
T101	121.3236	23.0203	−47.5	0.6	52.4	0.5	20.7	2.0	70.7	318
T102	121.2768	23.016	−41.0	0.6	55.2	0.5	41.4	1.6	68.8	323
T103	121.2674	23.155	−34.8	0.4	69.5	0.4	39.8	0.9	77.7	333
T104	121.2402	23.1548	−42.1	0.3	63.3	0.4	30.2	0.9	76.1	326
T105	121.2274	23.1555	−12.8	0.4	14.0	0.4	30.4	1.1	19.0	318
TAIP	121.6732	25.0345	2.4	0.2	1.9	0.2	−3.0	0.5	3.1	51
TANS	121.4269	25.1815	−2.5	0.5	0.2	0.4	−9.6	1.3	2.5	274
TATA	120.8871	23.4814	−20.9	0.2	5.0	0.2	20.7	2.0	21.5	284
TCMS	120.9874	24.798	−3.0	0.1	3.2	0.1	−1.6	0.1	4.4	317
TEGS	120.655	24.3562	−2.5	0.1	−0.6	0.1	−3.0	0.1	2.6	257
THAI	121.2956	24.6071	−4.1	0.1	11.7	0.1	2.6	0.1	12.4	341
TMAM	121.0075	22.6161	−34.3	0.3	10.9	0.2	−10.6	0.8	36.0	288
TOFN	120.9248	24.662	−6.5	0.3	3.9	0.2	2.1	0.6	7.6	301
TSHI	121.6328	25.2569	1.3	0.2	0.2	0.1	−2.1	0.4	1.3	82
TTUN	121.0807	22.7646	−39.0	0.2	11.1	0.2	0.3	0.6	40.5	286
TUCN	121.4961	24.5748	3.9	0.1	6.8	0.1	3.0	0.2	7.8	30
TUNM	121.4936	23.9652	−26.7	0.1	14.9	0.1	7.2	0.1	30.6	299
TUNS	120.404	23.3172	−12.6	0.2	1.9	0.1	3.0	0.5	12.8	278
TWTF	121.1645	24.9536	0.1	0.1	−0.6	0.1	0.3	0.1	0.6	168
WANC	120.5263	23.1868	−28.2	1.0	4.6	0.7	14.3	2.7	28.6	279
WANL	121.6376	25.1694	2.2	0.2	1.2	0.2	−1.7	0.4	2.5	60
WUKU	121.4007	25.1173	−0.1	0.1	2.5	0.1	−2.7	0.2	2.5	357
WUST	120.3682	23.2052	−13.2	0.1	−0.9	0.1	4.4	0.1	13.2	266
YAME	121.1853	24.9085	−2.8	0.1	3.4	0.1	2.3	0.2	4.4	320
YENL	121.6018	23.9035	−30.8	0.1	26.3	0.1	−10.1	0.1	40.5	310
YMSM	121.5741	25.1657	1.8	0.1	0.3	0.1	−2.5	0.1	1.8	79
YNTS	121.7789	24.8617	7.5	0.4	2.8	0.5	3.3	1.2	8.0	69
YSAN	120.086	23.1466	−4.7	0.3	−4.0	0.2	−7.6	0.6	6.1	230
YULI	121.3011	23.3409	−33.8	0.2	19.5	0.2	4.6	0.8	39.0	300
YUSN	120.9591	23.4873	−41.8	0.3	14.1	0.3	10.3	1.2	44.1	289

[a] V_N, V_E, and V_U are north, east and vertical component of average velocities, respectively. Err_N, Err_E, and Err_U are errors, respectively. V is average velocities of the horizontal component from January 2003 to December 2005. Azimuth is the azimuth angle.

pointed out that the south edge of the trough had been opening at a rate of 1.3 μrad/yr clockwise. During the two periods considered (1990–1995 and 2003–2005), clockwise rotation prevailed in the Ilan Plain region, whereas counterclockwise rotation affected the Pingtung Plain (Figures 9a and 9b). The Tainan region was, however, subject to a clockwise rotation that nearly equals that of the neighboring Pingtung Plain. This clockwise rotation is a probable consequence of the larger westward velocity of the southernmost fold-thrust units of the Western Foothills, as compared with the fold-thrust units of central south Taiwan. Rotations remain negligible, or marginally significant, in the other regions of the Eurasian portion of Taiwan.

[32] Some large amounts of counterclockwise rotation that apparently affect the eastern Central Range near 23°N and 23.5°N (Figures 9a and 9b) do not reflect the actual behavior of these areas but simply result from the distribution of the GPS stations. As no GPS station is present on the western edge of the Longitudinal Valley, the strain analysis is constrained by the stations of the eastern edge (in the fast moving Coastal Range) and a few stations at a large distance to the west inside the Central Range. As a result, because the strain determination by essence implies extrapolation and smoothing between the available GPS sites, a large deformation that occurs on the western edge of the Longitudinal Valley may "invade" large portions of the eastern edge. Such artifacts do not deserve consideration in the interpretation of strain maps.

[33] The largest rotation velocities are found in the Taitung region, with values up to −1.5 μrad/yr counterclockwise for both the pre- and post-Chi-Chi periods (Figures 9a and 9b). As an important difference, the northern boundary of this rotation area moved southward after the Chi-Chi earthquake.

[34] Another difference is the development of clockwise rotation along the eastern coast near 23°N during the post-Chi-Chi period, which accompanied a change from counterclockwise to clockwise before and after event 1 (compare Figures 9c and 9d). Long-term clockwise rotations accompanied the collision of the major units of the Luzon arc against the Chinese margin since about 2 Ma, as documented from paleomagnetic studies [*Lee*, 1994; *Lee et al.*, 1991]. In the eastern coastal area near 23°N, the comparison between Figures 9c and 9d probably highlights the contrast between a slow permanent counterclockwise rotation (also indicated by Figure 9a) and the large postseismic clockwise rotation of an arc block after the Chengkung earthquake.

4. Discussion and Summary

4.1. Coseismic and Postseismic Disturbance in the Time Period 2003–2005

[35] The main goal of this paper is to elucidate the active deformation in the active Taiwan orogenic belt after the

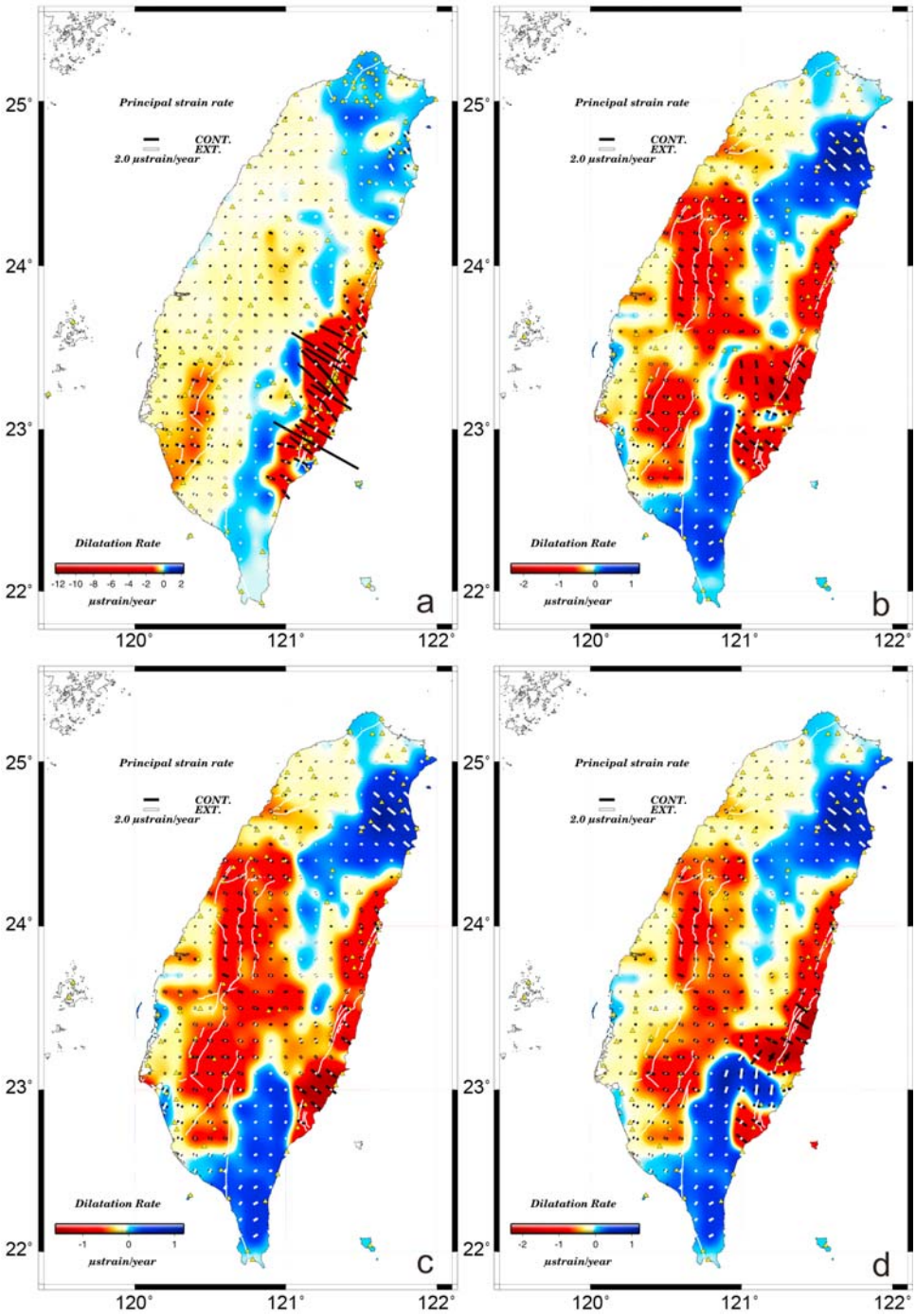

Figure 8. Horizontal principal axes of strain rates. The amount and direction of principal strain rates are shown by arrows. Triangles are locations of GPS sites. The color scale shows magnitudes of dilatation rates. (a) Period 1990–1995, from Figure 2. (b) Data analysis from 1 January 2003 to 31 December 2005. (c) Data analysis from 1 January 2003 to 10 December 2003. (d) Data analysis from 11 December 2003 to 5 March 2005.

1999 Chi-Chi earthquake. The results of CGPS show that the hanging wall of the Chelungpu fault is still moving northwestward with the velocities of 18.1–45.5 mm/yr, which are larger than the station velocities of 5–11.8 mm/yr observed by the campaign mode GPS survey. It implies that postseismic processes were still active during 2003–2005. Recently, *Savage et al.* [2005] proposed that the initial ($t < 0.1$ year) postseismic deformation were well fit by $\log(t)$ dependence associated with transient (primary) creep following by 1992 Landers, 1999 Chi-Chi, 1999 Hector Mine, 2002 Denali, 2003 San Simeon, and 2004 Parkfield earthquakes. The postseismic displacement of as much as 14 cm was recorded by GPS survey in the 3 months following the Chi-Chi earthquake [*Hsu et al.*, 2002]. The fits to an

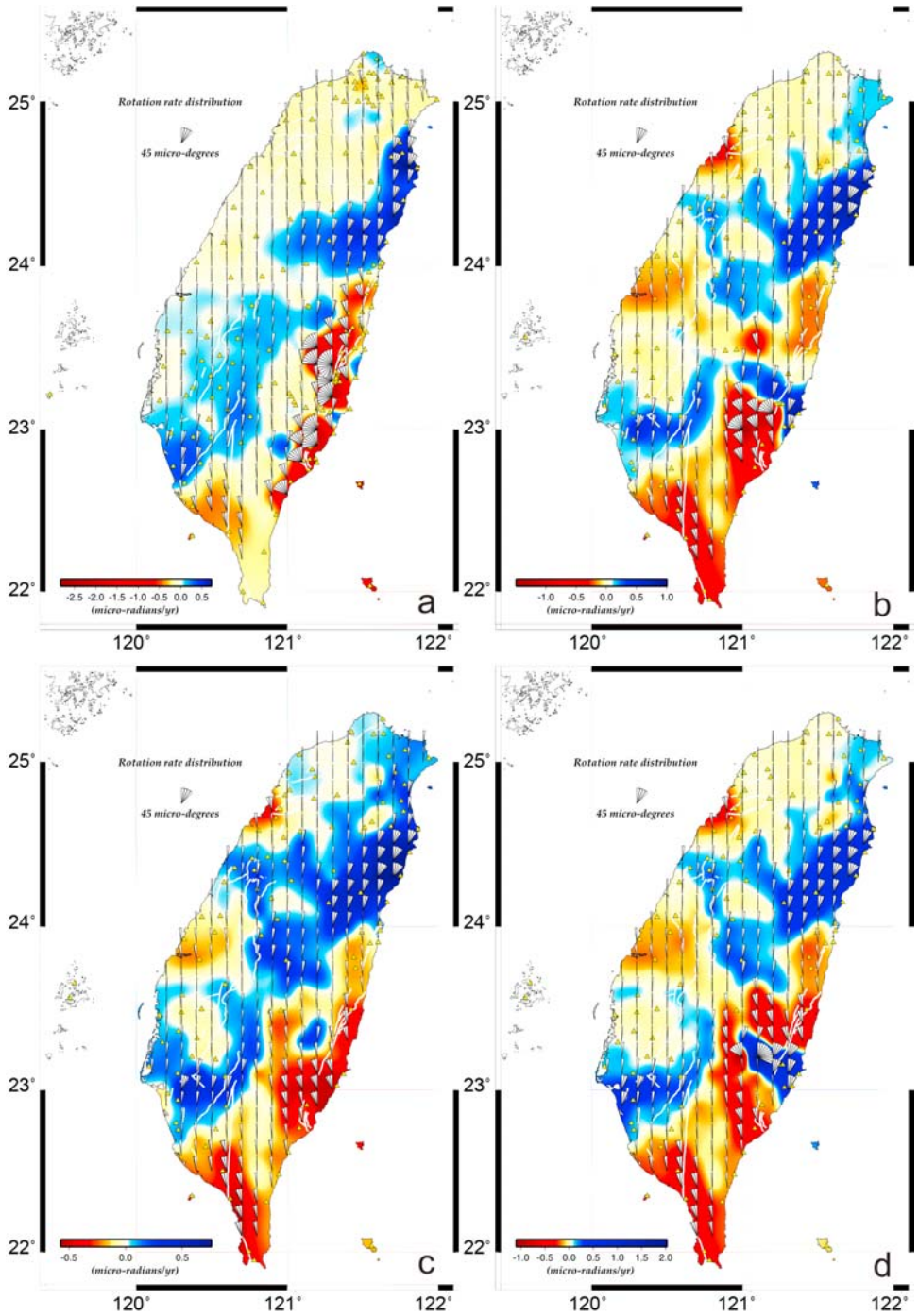

Figure 9. Rotation amounts indicated by GPS data. (a) Period 1990–1995, from Figure 2. (b) Data analysis from 1 January 2003 to 31 December 2005. (c) Data analysis from 1 January 2003 to 10 December 2003. (d) Data analysis from 11 December 2003 to 5 March 2005.

exponential decay of six stations in the hanging wall were done for the postseismic displacements for this specified time interval [*Hsu et al.*, 2002]. The postseismic displacement was predicted by the rapid afterslip of 25 cm in the hypercentral region at 7–12 km and significant slip on the lower décollement. In a 15 month period, *Yu et al.* [2003] used equation (1) to model the observed postseismic displacement $Y(t_i)$ of CGPS station in each direction after Chi-Chi earthquake. The postseismic displacement was approximated by a combination of an exponential transient decay function with a relaxation time of 86 days and a postseismic linear rate change [*Yu et al.*, 2003]. In addition, a test had been done to evaluate whether postseismic deformation was better predicted by afterslip or viscoelastic relaxation of the lower crust and upper mantle on the basis of GPS displacement in a 15 month period after the Chi-Chi earthquake [*Hsu et al.*, 2007]. They used a three-layer model that included an elastic upper crust at 0–20 km, a

viscoelastic lower crust with viscosity 10^{18} Pa s from 20 to 40 km depth, and a viscoelastic upper mangle with viscosity of 10^{20} Pa s at depth >40 km. They concluded that all viscoelastic models tested fail to fit the general features in the postseismic GPS displacement but fit quite well with afterslip model. Furthermore, an azimuthal difference of about 10°–20° between preseismic and postseismic GPS velocities was reported by *Hsu et al.* [2009c]; they inferred that the very low shear stress on the creeping portion of the décollement beneath the Central Range [*Hsu et al.*, 2009c]. *Perfettini and Avouac* [2004] proposed a possible mechanism of postseismic relaxation driven by a brittle creep in the brittle creeping fault zone on the basis of the observation of geodetic measurements and the decay rate of aftershocks. This model predicted an initial logarithmic increase of slip with time. The inferred relaxation time is rate dependent. An inferred relaxation time of 8.5 years required a value of $a = \partial\mu/\partial \log(V)$ in the rage between 1.3×10^{-3} and $\times 10^{-2}$. They proposed that the postseismic relaxation does involve viscous flow at greater depth and fluid flow redistribution within the upper crust but the brittle creep mechanism should operate concurrently. Thus, a fraction of the signal of GPS displacement that we have observed at present might be due to a viscoelastic response rather than afterslip which dominated the signal initially (J.-P. Avouac, personal communication, 2009). To first order the strain field due to the viscoelastic response should look like an accelerated version of the preseismic strain field; this will be checked in the further study of numerical simulation.

[36] In the case of postseismic deformation after the 2003 Chengkung earthquake, *Savage and Yu* [2007] demonstrated that the postseismic relaxation and aftershocks were driven by fault slip on the coseismic rupture. They also proposed that the afterslip seemed to be the primary contribution to the postseismic deformation and the Chihshang fault also contributed shallow creep after the main shock. *Hsu et al.* [2009b] suggested that the postseismic slip of ~0.1 m over a 157 day period occurred at a depth of 15 km. On the basis of continuously recording GPS stations, a largest relaxation time of 87 days was proposed [*Chen et al.*, 2006]. However, the large postseismic displacements in 18 months approached 86 mm (station SHAN) and 91 mm (station TAPO) in the horizontal and vertical components, respectively [*Chen et al.*, 2006]. To estimate the secular crustal deformation during the period after the Chengkung event, the temporal variations can be computed by equation (1); thus, the secular crustal movement after earthquake and the relaxation time can be estimated from the position variations.

4.2. Displacement Patterns Before and After the Chi-Chi Earthquake

[37] As the very large 1999 Chi-Chi earthquake (M_w = 7.6) occurred between the major survey periods, it is interesting to compare the average velocity patterns of those periods, 1990–1995 [*Yu et al.*, 1997] and 2003–2005. This comparison is presented in Figure 10; Figure 10c presents both the successive displacement patterns and their vector difference field.

[38] In regions like northernmost Taiwan for small velocities and Lutao Island for high velocities, the differences are not significant, or even marginally significant. The largest differences occur in central Taiwan, where westward velocities dramatically increased after the Chi-Chi earthquake as a result of lower mechanical coupling during the postseismic period with respect to the preseismic situation. In an area about 80 km wide and 100 km long of the Central Range and foothills, velocities increased by up to 20–25 mm/yr with respect to the preseismic period (Figure 10c).

[39] In the foothill region of Chiayi and Tainan and the Central Range adjacent to it, differences in velocity are negligible (Figure 10c), suggesting that the mechanical coupling is the same as before the Chi-Chi-earthquake. This vector difference pattern is consistent with an abrupt, across-belt change between a central domain (shown as a dark gray pattern in Figure 10d) affected by the major earthquake that shows contrasting seismic and postseismic deformation patterns, and the other two domains (light gray pattern in Figure 10d) where little or no change has occurred.

[40] Significant, albeit less pronounced, changes took place in and around the Ilan and Pingtung plains. In these domains dominated by extrusion at both tips of the collision belt [*Angelier et al.*, 2009], a significant increase in average velocity, up to 10–15 mm/yr, suggests that extrusion toward east and southeast (off Ilan) or southwest (off Pingtung) was more active after than before the Chichi earthquake (Figure 8d). A minor but significant counterclockwise change in the direction of relative displacement has also affected the Coastal Range, resulting in southward directed difference vectors along the coast of southern Taiwan (Figure 10d).

[41] The analysis of the successive patterns of horizontal displacement vectors, before and after the 1999 Chi-chi earthquake, thus reveals a major change dominated by increasing heterogeneity in displacement along the Taiwan belt, with a quick westward displacement in the previously locked domain (as shown by different vectors in Figure 10c). Six main domains are thus distinguished in Figure 8d as far as the velocity pattern is concerned: domains showing limited changes (light gray pattern) (domains 1 and 2), major increase in displacement toward south China (dark gray pattern) (domain 3), lateral escape and extrusion toward the adjacent subduction zones near belt tips (dashed lines) (domains 4 and 5), and across-suture shortening associated with minor deviation suggesting a limited southward escape (dotted line) near the southern corner of the region that experienced major velocity increase after the Chi-Chi earthquake (domain 6).

4.3. Temporal Variation of Crustal Strain Rate in Taiwan

[42] Figure 11a shows the differences between the strain patterns of two different periods: 1990–1995 and 2003–2005, revealing strong contrasts in the domains affected by the Chi-Chi earthquake. On the contrary, the presence of small positive values of dilatation rate in the high Central Range of Taiwan, between two domains where shortening prevailed, is another constant feature (Figure 8, all maps). During the postseismic period, shortening at rates of about 0.5–1 μstrain/yr in an ENE–WSW direction developed in a large area of the foothills and western Central Range of Taiwan, where smaller rates (around 0.5–1 μstrain/yr) pre-

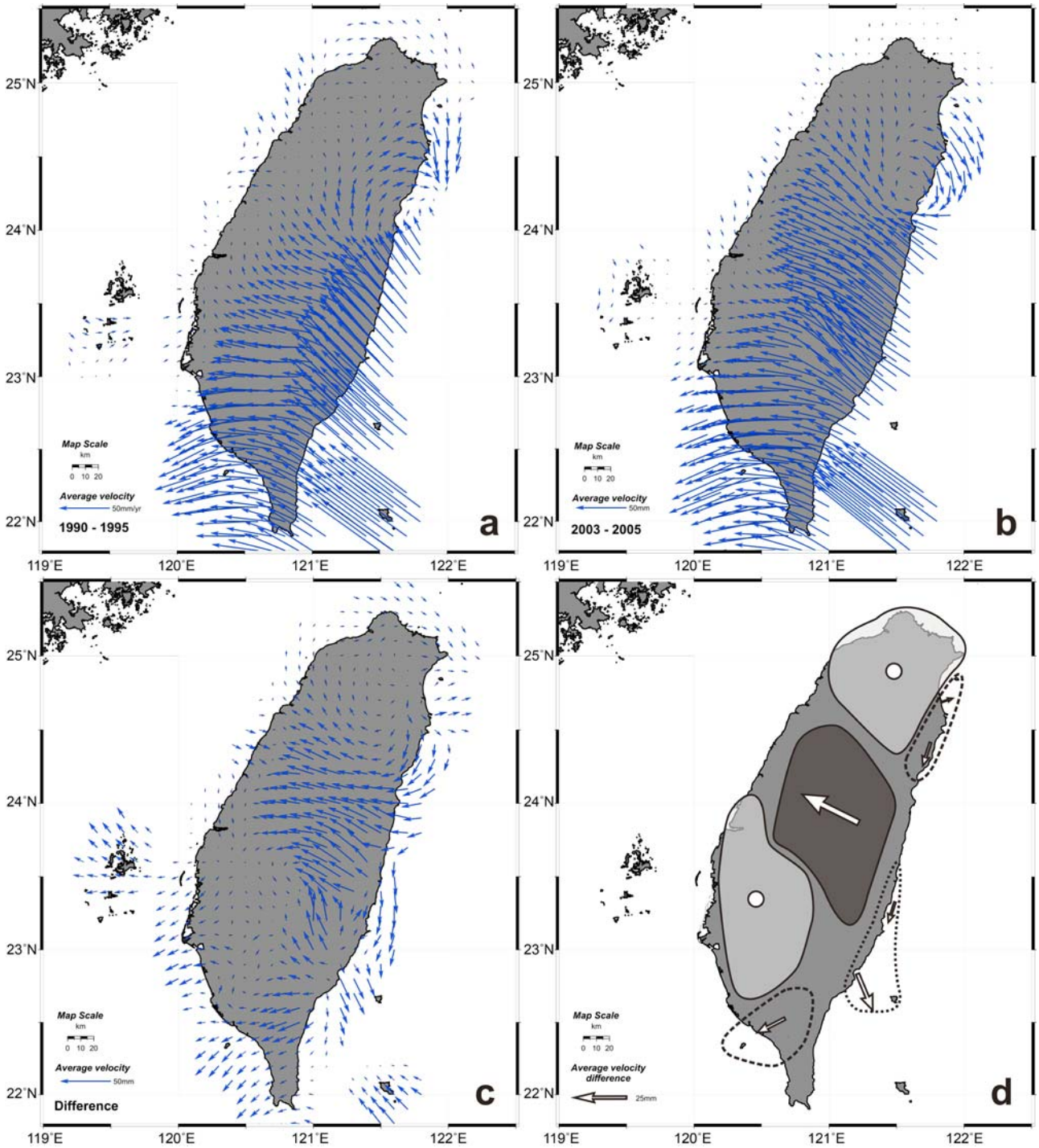

Figure 10. Comparison between the displacement velocity patterns interpolated throughout Taiwan based on GPS data from two periods before and after the Chi-Chi earthquake sequence: (a) 1990–1995 [*Yu et al.*, 1997] and (b) 2003–2005. Figures 10a and 10b present grid interpolations from the local data of Figures 2 and 7, respectively. (c) Resulting vector difference patterns (in terms of annual average velocity). (d) Major domains with characteristic behaviors regarding the change from Figures 10a to 10b. Average displacement velocities are shown as white arrows (and white circles in the absence of significant change). Light gray areas indicate domains with very similar kinematic behavior. Dark gray areas indicate the domain with a major increase in velocity ranging from the preseismic to postseismic periods. Dashed lines indicate the portion of extrusion domains showing velocity change at belt tips. Dotted line demarks the southern half of the Coastal Range of eastern Taiwan.

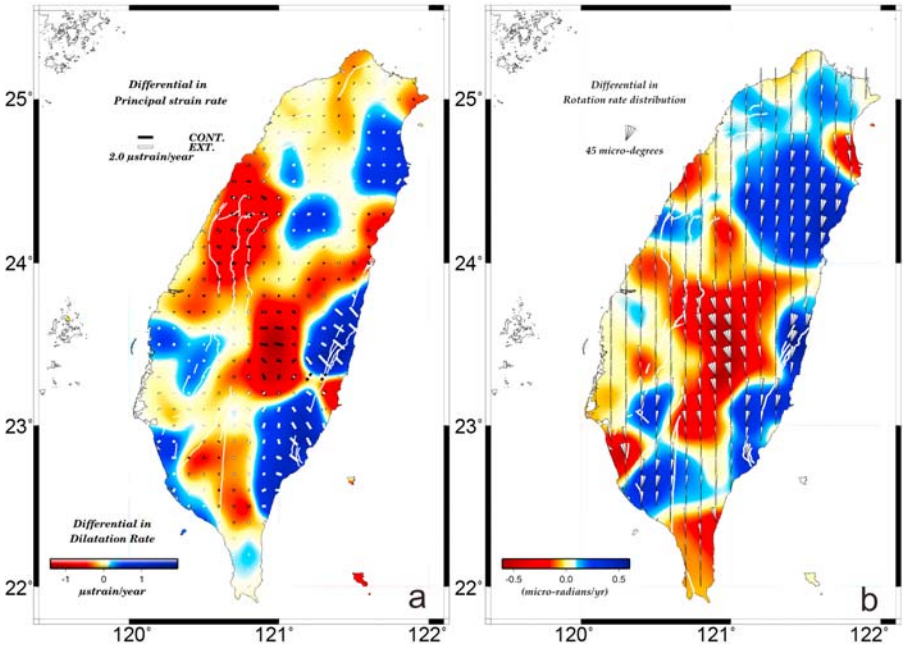

Figure 11. (a) The difference in principal strain rate and (b) difference in rotation rate before and after Chi-Chi earthquake (1990–1995 and 2003–2005).

vailed in 1990–1995. Such changes are highlighted by differences in displacement (Figures 10c and 10d) and strain rate (Figure 11a).

[43] The Chengkung earthquake, albeit less important, had significant impact on the GPS records. Comparing our recording periods before and after event 1 (Figures 8c and 8d), large variations in strain rate patterns took place in the southern Coastal Range area affected by the Chengkung earthquake, where dilatation with values of about 1 μstrain/yr replaced shortening with values around -1 μstrain/yr (blue and red, respectively, compare Figures 8c and 8d). Likewise, large change in rotations occurred in this area (compare Figures 9c and 9d). Other variations throughout Taiwan were minor.

[44] These two comparisons highlight the large difference in spatial extent between the regional strain changes related to the $M_w = 7.6$ Chi-Chi earthquake (Figures 8a and 8b) and the more local ones accompanying the $M_w = 6.8$ Chengkung earthquake (Figures 8c and 8d). Interestingly, the rotation changes were larger in the second case, consistent with the limited width of the block affected by the thrusting in the crust.

4.4. Summary of Geodetic Results and Insights for Seismic Activity

[45] In so far as discussion can be drawn from GPS data acquisition since 1990, including the continuous recording at many stations since 2003, some major aspects of displacement and deformation in Taiwan should be regarded as characteristic of longer-term tectonism, in agreement with a variety of geological observations. They include the NW–SE convergence and shortening across the collision zone (especially at and east of two major active boundaries, the Longitudinal Valley to the east and the belt front to the west), the extrusion at belt tips (Ilan Plain to the northeast, Pingtung Plain to the southwest), and the presence of extension in the Central Range.

[46] However, these data also show that significant changes in displacement, strain rate, and rotation occur during large earthquakes. Not only did the Chi-Chi earthquake reveal the importance of the west Taiwan tectonic boundary in the structural frame of Taiwan [*Angelier et al.*, 2001], it also induced important changes in the distribution of displacement and strain in the island. As a consequence of the earthquake cycle near the front of the orogen, the difference between the patterns of displacement and strain was quite significant. As an example of postseismic relaxation and after slip, consistent with coseismic behavior of the hanging wall [*Chang et al.*, 2003], the six stations located in the upthrust block of the Chelungpu Fault had velocities of 18.1–45.5 mm/yr with directions 286°–296° from 2003 to 2005, much larger than before the Chi-Chi earthquake, documented at three survey mode geodetic monuments: S032 (5.0 ± 1.9 mm/yr, azimuth 329° ± 2°), HTZS (11.8 ± 2 mm/yr, 310° ± 2°), and JEFS (11.4 ± 2.1 mm/yr, 328.7° ± 2°) from 1990 to 1995 [*Yu et al.*, 1997].

[47] In contrast, the Chengkung and Hualien earthquakes did not markedly affect the island-wide pattern of displacement and strain. These earthquakes occurred at the active tectonic boundary in Taiwan where the last major events were the Hualien-Yuli-Taitung earthquakes of 1951. The absence of a very large event in eastern Taiwan during the GPS recording period precludes direct comparison between their displacement-strain behaviors as a function of the earthquake cycle.

5. Conclusion

[48] We use 3 years of continuous GPS to estimate the velocities from 2003 to 2005. With respect to Paisha station,

S01R, the stations of Coastal Range and Lanhsu showed an average displacement of 40.5–93.6 mm/yr with directions of 307°–333°. The stations in the Longitudinal Valley and Central Range revealed velocities in the range 19.0–49.3 mm/yr with directions of 285°–318°. In western Taiwan, the velocities in the inner fold-and-thrust belt range from 14.2 to 45.5 mm/yr with directions of 284°–304°. Significant postseismic deformation after the Chi-Chi earthquake was detected in central Taiwan with a major increase in displacement velocity toward south China.

[49] Despite the influence of the Chi-Chi earthquake on the displacement and strain patterns, scale ranges in the difference maps for strain and rotation reach 3.3 μstrain/yr and 2.3 μrad/yr, respectively, as compared with 4 μstrain/yr and more and 2–3.5 μrad/yr in the preseismic and postseismic pattern maps, respectively. This comparison shows that the changes in the distribution of strain and rotation induced by this very large earthquake remained smaller than, albeit of the same order as, the corresponding contrasts that prevailed throughout Taiwan before and after.

[50] In contrast, the Chengkung earthquake did not markedly affect the island-wide pattern of displacement and strain. However, it resulted in major changes in strain and block rotation at a more local scale than the Chi-Chi earthquake, i.e., at the scale of the southern Coastal Range. Despite its relatively limited magnitude, this Chengkung earthquake clearly affected shortening on the opposite, western side of the southern collision belt at station TUNS.

[51] Regarding earthquakes with lower magnitudes, such as the Ilan double earthquakes and the Hualien earthquake, their impact on the displacement and strain patterns was not negligible but remained local. These results show that although large and medium size earthquakes affect the GPS strain pattern. They do this, however, in different ways: regional extension and displacement were large, while rotations were minor for the large, M_w = 7.6 Chi-Chi earthquake. In contrast, extension was limited, displacement was moderate, and rotations were large for the 2003 M_w = 6.8 Chengkung earthquake. Regarding smaller earthquakes such as the 2005 M_w = 5.9 Ilan double earthquakes and the 2005 M_w = 5.6 Hualien earthquake, their impact on the deformation is locally significant but regionally minor.

[52] The GPS data provide a snapshot of the deformation that is generally consistent with the long-term history of the collision, although it should be considered with caution as thrust deformation moves through time along the tectonic boundary. The kinematic changes resulting from the smallest events remain mainly local. For the largest event, the Chi-Chi earthquake, the new GPS data show that the Chi-Chi hanging wall is still recognizable as a kinematic block, in contrast to the previous pattern in which the hanging wall was not discernable.

[53] **Acknowledgments.** The comments and suggestions from Editor Patrick Taylor and four anonymous reviewers are deeply appreciated. We also benefit from the discussion with Jean-Philippe Avouac. We are grateful to the Satellite Survey Center, Department of Land Administration, MOI; Department of Earth Sciences, National Cheng Kung University; Department of Geosciences, National Taiwan University; and Central Weather Bureau for offering continuous GPS observations. J.A.'s research was supported by the Institut Universitaire de France. We benefited greatly by the establishment of continuous GPS stations and the experience of data processing from the Institute of Earth Sciences, Academia Sinica, and Central Weather Bureau.

References

Altamimi, Z., P. Sillard, and C. Boucher (2002), ITRF2000: A new release of the International Terrestrial Reference Frame for earth science applications, *J. Geophys. Res.*, *107*(B10), 2214, doi:10.1029/2001JB000561.

Angelier, J., H.-T. Chu, and J.-C. Lee (1997), Shear concentration in a collision zone: Kinematics of the active Chihshang Fault, Longitudinal Valley, eastern Taiwan, *Tectonophysics*, *274*, 117–143, doi:10.1016/S0040-1951(96)00301-0.

Angelier, J., H.-T. Chu, J.-C. Lee, and J.-C. Hu (2000), Active faulting and earthquake risk: The Chihshang Fault case, Taiwan, *J. Geodyn.*, *29*, 151–185, doi:10.1016/S0264-3707(99)00045-9.

Angelier, J., J.-C. Lee, H.-T. Chu, J.-C. Hu, C.-Y. Lu, Y.-C. Chan, T.-J. Lin, Y. Font, B. Deffontaines, and Y.-B. Tsai (2001), Le séisme de Chichi (1999) et sa place dans l'orogène de Taiwan, *C. R. Acad. Sci., Ser. IIa*, *333*, 1, 5–21.

Angelier, J., T.-Y. Chang, J.-C. Hu, C.-P. Chang, L. Siame, J.-C. Lee, B. Deffontaines, H.-T. Chu, and C.-Y. Lu (2009), Does extrusion occur at both tips of the Taiwan collision belt? Insights from active deformation studies in the Ilan Plain and Pingtung Plain regions, *Tectonophysics*, *466*, 356–376, doi:10.1016/j.tecto.2007.11.015.

Brunner, F. K., and W. M. Welsch (1993), Effects of the troposphere on GPS measurements, *GPS World*, *4*, 42–51.

Carena, S., J. Suppe, and H. Kao (2002), Active detachment of Taiwan illuminated by small earthquakes and its control of first-order topography, *Geology*, *30*, 935–938, doi:10.1130/0091-7613(2002)030<0935:ADOTIB>2.0.CO;2.

Chang, C.-P., T.-Y. Chang, J. Angelier, H. Kao, J.-C. Lee, and S.-B. Yu (2003), Strain and stress field in Taiwan oblique convergent system: Constraints from GPS observation and tectonic data, *Earth Planet. Sci. Lett.*, *214*, 115–127, doi:10.1016/S0012-821X(03)00360-1.

Chen, H.-Y., S.-B. Yu, L.-C. Kuo, and C.-C. Liu (2006), Coseismic and postseismic displacement of the 10 December 2003(M_w 6.5) Chengkung earthquake, eastern Taiwan, *Earth Planets Space*, *58*, 5–21.

Cheng, L.-W., J.-C. Lee, J.-C. Hu, and H.-Y. Chen (2009), Coseismic and postseismic slip distribution of the 2003 M_w = 6.5 Chengkung earthquake in eastern Taiwan: Elastic modeling from inversion of GPS data, *Tectonophysics*, *466*, 335–343, doi:10.1016/j.tecto.2007.11.021.

Ching, K.-E., R.-J. Rau, J.-C. Lee, and J.-C. Hu (2007), Contemporary deformation of tectonic escape in SW Taiwan from GPS observations, 1995–2005, *Earth Planet. Sci. Lett.*, *262*, 601–619, doi:10.1016/j.epsl.2007.08.017.

Deffontaines, B., O. Lacombe, J. Angelier, F. Mouthereau, C.-T. Lee, J. Deramond, J.-F. Lee, M.-S. Yu, and P.-M. Liu (1997), Quaternary transfer faulting in Taiwan Foothills: Evidence from a multisource approach, *Tectonophysics*, *274*, 61–82, doi:10.1016/S0040-1951(96)00298-3.

Dixon, T. H. (1991), An introduction to the Global Positioning System and some geological applications, *Rev. Geophys.*, *29*, 249–276, doi:10.1029/91RG00152.

Frank, F. C. (1966), Deduction of Earth strains from survey data, *Bull. Seismol. Soc. Am.*, *56*, 35–42.

Ho, C.-S. (1986), A synthesis of the geological evolution of Taiwan, *Tectonophysics*, *125*, 1–16, doi:10.1016/0040-1951(86)90004-1.

Hou, C.-S., J.-C. Hu, Y.-G. Chen, C.-L. Chen, L.-W. Cheng, C.-L. Tang, S.-H. Huang, and C.-H. Lo (2009), The crustal deformation of the Ilan Plain acted as a westernmost extension of the Okinawa Trough, *Tectonophysics*, *466*, 344–355, doi:10.1016/j.tecto.2007.11.022.

Hsu, Y.-J., N. Bechor, P. Segall, S.-B. Yu, L.-C. Kuo, and K.-F. Ma (2002), Rapid afterslip following the 1999 Chi-Chi, Taiwan, earthquake, *Geophys. Res. Lett.*, *29*(16), 1754, doi:10.1029/2002GL014967.

Hsu, Y.-J., M. Simons, S.-B. Yu, L.-C. Kuo, and H.-Y. Chen (2003), A two-dimensional dislocation model for interseismic deformation of the Taiwan mountain belt, *Earth Planet. Sci. Lett.*, *211*, 287–294, doi:10.1016/S0012-821X(03)00203-6.

Hsu, Y.-J., P. Segall, S.-B. Yu, L.-C. Kuo, and C. A. Williams (2007), Temporal and spatial variations of postseismic deformation following the 1999 Chi-Chi, Taiwan earthquake, *Geophys. J. Int.*, *169*, 367–379, doi:10.1111/j.1365-246X.2006.03310.x.

Hsu, Y.-J., S.-B. Yu, M. Simons, L.-C. Kuo, and H.-Y. Chen (2009a), Interseismic crustal deformation in the Taiwan plate boundary zone revealed by GPS observations, seismicity, and earthquake focal mechanisms, *Tectonophysics*, *479*, 4–18, doi:10.1016/j.tecto.2008.11.016.

Hsu, Y.-J., S.-B. Yu, and H.-Y. Chen (2009b), Coseismic and postseismic deformation associated with the 2003 Chengkung, Taiwan earthquake, *Geophys. J. Int.*, *176*, 420–430, doi:10.1111/j.1365-246X.2008.04009.x.

Hsu, Y.-J., J.-P. Avouac, S.-B. Yu, C.-H. Chang, Y.-M. Wu, and J. Woessner (2009c), Spatio-temporal slip, and stress level on the faults within western Foothills of Taiwan: Implication for fault frictional properties, *Pure Appl. Geophys.*, *166*, 1853–1884, doi:10.1007/s00024-009-0510-5.

Hu, J.-C., J. Angelier, J.-C. Lee, H.-T. Chu, and D. Byrne (1996), Kinematics of convergence, deformation and stress distribution in the Taiwan collision area: 2-D finite-element numerical modeling, *Tectonophysics*, *255*, 243–268, doi:10.1016/0040-1951(95)00140-9.

Hu, J.-C., J. Angelier, and S.-B. Yu (1997), An interpretation of the active deformation of southern Taiwan based on numerical simulation and GPS studies, *Tectonophysics*, *274*, 145–169, doi:10.1016/S0040-1951(96)00302-2.

Hu, J.-C., S.-B. Yu, J. Angelier, and H.-T. Chu (2001), Active deformation of Taiwan from GPS measurements and numerical simulations, *J. Geophys. Res.*, *106*, 2265–2280, doi:10.1029/2000JB900196.

Hu, J.-C., S.-B. Yu, H.-T. Chu, and J. Angelier (2002), Transition tectonics of northern Taiwan induced by convergence and trench retreat, in *Geology and Geophysics of an Arc-Continent Collision, Taiwan*, edited by T. B. Byrne and C.-S. Liu, *Spec. Pap. Geol. Soc. Am.*, 358, 149–162.

Hu, J.-C., H.-T. Chu, C.-S. Hou, R.-F. Chen, T.-H. Lai, and P.-F. Nien (2006), The contribution to tectonic subsidence by groundwater abstraction in the Pingtung area, southwestern Taiwan as determined by GPS measurements, *Quat. Int.*, *147*, 62–69, doi:10.1016/j.quaint.2005.09.007.

Hu, J.-C., et al. (2007), Coseismic deformation revealed by inversion of strong motion and GPS data: The 2003 Chengkung earthquake in eastern Taiwan, *Geophys. J. Int.*, *169*, 667–674, doi:10.1111/j.1365-246X.2007.03359.x.

Hugentobler, U., S. Schaer, and P. Fridez (Eds.) (2001), Bernese GPS software, version 4.2, 515 pp., Astron. Inst., Univ. of Berne, Bern, Switzerland.

Johnson, K. M., and P. Segall (2004), Imaging the ramp-décollement geometry of the Chelungpu fault using coseismic GPS displacements from the 1999 Chi-Chi, Taiwan earthquake, *Tectonophysics*, *378*(1–2), 123–139, doi:10.1016/j.tecto.2003.10.020.

Johnson, K. M., and P. Segall (2005), A viscoelastic earthquake cycle model for Taiwan, *J. Geophys. Res.*, *110*, B10404, doi:10.1029/2004JB003516.

Lacombe, O., F. Mouthereau, J. Angelier, and B. Deffontaines (2001), Structural, geodetic and seismological evidence for tectonic escape in SW Taiwan, *Tectonophysics*, *333*, 323–345, doi:10.1016/S0040-1951(00)00281-X.

Lee, J.-C. (1994), Structure et déformation active d'un orogène: Taiwan, *Mem. Sci. Terre 94-17*, 328 pp., Univ. P. et M. Curie, Paris.

Lee, J.-C., J. Angelier, H.-T. Chu, J.-C. Hu, F.-S. Jeng, and R.-J. Rau (2003), Active fault creep variations at Chihshang, Taiwan, revealed by creepmeter monitoring, 1998–2001, *J. Geophys. Res.*, *108*(B11), 2528, doi:10.1029/2003JB002394.

Lee, J.-C., H.-T. Chu, J. Angelier, J.-C. Hu, H.-Y. Chen, and S.-B. Yu (2006), Quantitative analysis of co-seismic surface faulting and post-seismic creep accompanying the 2003, M_w = 6.5, Chengkung earthquake in eastern Taiwan, *J. Geophys. Res.*, *111*, B02405, doi:10.1029/2005JB003612.

Lee, T.-Q., C. Kissel, E. Barrier, C. Laj, and W.-R. Chi (1991), Paleomagnetic evidence for a diachronic clockwise rotation of the Coastal Range, eastern Taiwan, *Earth Planet. Sci. Lett.*, *104*, 245–257, doi:10.1016/0012-821X(91)90207-X.

Letouzey, J., and M. Kimura (1985), Okinawa Trough genesis: Structure and evolution of a back-arc basin developed in a continent, *Mar. Pet. Geol.*, *2*, 111–130, doi:10.1016/0264-8172(85)90002-9.

Lin, C.-W., H.-C. Chang, S.-T. Lu, T.-S. Shih, and W.-C. Huang (2000), An introduction to the active faults of Taiwan: Explanatory text of the active fault map of Taiwan (in Chinese), 2nd ed., scale 1:500,000, *Spec. Publ. 13*, 122 pp., Cent. Geol. Surv., Taipei, Taiwan.

Lin, K.-C., K.-E. Ching, J.-C. Hu, T.-T. Yu, and R.-J. Rau (2006), Current crustal deformation and strain rate in Taiwan deduced from continuous GPS measurements, *Geophys. Res. Abstr.*, *8*, 07,160.

Liu, C.-C. (1995), The Ilan Plain and the southwestward extending Okinawa Trough, *J. Geol. Soc. China*, *38*, 229–242.

Nikolaidis, R. (2002), Observation of geodetic and seismic deformation with the Global Positioning System, Ph.D. dissertation, 249 pp., Univ. of Calif., San Diego, La Jolla.

Pathier, E., B. Fruneau, B. Deffontaines, J. Angelier, C.-P. Chang, S.-B. Yu, and C.-T. Lee (2003), Coseismic displacements of the footwall of the Chelungpu fault caused by the 1999, Taiwan, Chi-Chi earthquake from InSAR and GPS data, *Earth Planet. Sci. Lett.*, *212*, 73–88, doi:10.1016/S0012-821X(03)00244-9.

Perfettini, H., and J.-P. Avouac (2004), Postseismic relaxation driven by brittle creep: A possible mechanism to reconcile geodetic measurements and the decay rate of aftershocks, application to the Chi-Chi earthquake, Taiwan, *J. Geophys. Res.*, *109*, B02304, doi:10.1029/2003JB002488.

Prescott, W. H. (1976), An extension of Frank's method for obtaining crustal shear strain from survey data, *Bull. Seismol. Soc. Am.*, *66*, 1847–1853.

Rau, R.-J., K.-E. Ching, J.-C. Hu, and J.-C. Lee (2008), Crustal deformation and block kinematics in transition from collision to subduction: Global positioning system measurements in northern Taiwan, 1995–2005, *J. Geophys. Res.*, *113*, B09404, doi:10.1029/2007JB005414.

Saastamoinen, I. I. (1973), Contribution to the theory of atmospheric refraction, *Bull. Geod.*, *107*, 13–34, doi:10.1007/BF02522083.

Savage, J. C., and S.-B. Yu (2007), Postearthquake relaxation and aftershock accumulation linearly relatd after the 2003 M 6.5 Chengkung, Taiwan and the 2004 M 6.0 Parkfield, California, earthquakes, *Bull. Seismol. Soc. Am.*, *97*, 1632–1645, doi:10.1785/0120070069.

Savage, J. C., J. L. Svarc, and S.-B. Yu (2005), Postseismic relaxation and transient creep, *J. Geophys. Res.*, *110*, B11402, doi:10.1029/2005JB003687.

Segall, P., and J. L. Davis (1997), GPS applications for geodynamics and earthquake studies, *Annu. Rev. Earth Planet. Sci.*, *25*, 301–336, doi:10.1146/annurev.earth.25.1.301.

Seno, T., S. Stein, and A. E. Gripp (1993), A model for the motion of the Philippine Sea plate consistent with NUVEL-1 and geological data, *J. Geophys. Res.*, *98*, 17,941–17,948, doi:10.1029/93JB00782.

Shen, Z. K., D. D. Jackson, and B. X. Ge (1996), Crustal deformation across and beyond the Los Angeles basin from geodetic measurements, *J. Geophys. Res.*, *101*, 27,957–27,980, doi:10.1029/96JB02544.

Sibuet, J. C., et al. (1987), Back-arc extension in the Okinawa Trough, *J. Geophys. Res.*, *92*(B13), 14,041–14,063, doi:10.1029/JB092iB13p14041.

Suppe, J. (1980), Imbricated structure of western Foothills belt, south-central Taiwan, *Petrol. Geol. Taiwan*, *17*, 1–16.

Suppe, J. (1984), Kinematics of arc–continent collision, flipping of subduction and back-arc spreading near Taiwan, *Mem. Geol. Soc. China*, *6*, 21–33.

Tabei, T., and W. L. Amin (2002), Common-mode errors in the GPS coordinates time series: Application of spatial filtering technique, *J. Geod. Soc. Jpn.*, *48*, 229–241.

Thatcher, W. (2003), GPS constraints on the kinematics of continental deformation, *Int. Geol. Rev.*, *45*(3), 191–212, doi:10.2747/0020-6814.45.3.191.

Tsai, Y.-B. (1986), Seismotectonics of Taiwan, *Tectonophysics*, *125*, 17–37, doi:10.1016/0040-1951(86)90005-3.

Wang, C.-Y., and T.-C. Shin (1998), Illustrating 100 years of Taiwan seismicity, *Terr. Atmos. Oceanic Sci.*, *9*, 589–614.

Ward, S. N. (1994), A multidisciplinary approach to seismic hazard in southern California, *Bull. Seismol. Soc. Am.*, *84*, 1293–1309.

Wdowinski, S., Y. Bock, J. Zhang, P. Fang, and J. Genrich (1997), Southern California permanent GPS geodetic array: Spatial filtering of daily positions for estimating coseismic and postseismic displacements induced by the 1992 Landers earthquake, *J. Geophys. Res.*, *102*, 18,057–18,070, doi:10.1029/97JB01378.

Yang, M., R.-J. Rau, J.-Y. Yu, and T.-T. Yu (2000), Geodetically observed surface displacements of the 1999 Chi-Chi, Taiwan, earthquake, *Earth Planets Space*, *52*, 403–413.

Yu, S.-B., and L.-C. Kuo (2001), Present-day crustal motion along the Longitudinal Valley fault, eastern Taiwan, *Tectonophysics*, *333*, 199–217, doi:10.1016/S0040-1951(00)00275-4.

Yu, S.-B., H.-Y. Chen, and L.-C. Kuo (1997), Velocity field of GPS Stations in the Taiwan area, *Tectonophysics*, *274*, 41–59, doi:10.1016/S0040-1951(96)00297-1.

Yu, S.-B., L.-C. Kuo, R. S. Punongbayan, and E. G. Ramos (1999), GPS observation of crustal deformation in the Taiwan-Luzon region, *Geophys. Res. Lett.*, *26*, 923–926, doi:10.1029/1999GL900148.

Yu, S.-B., et al. (2001), Preseismic deformation and coseismic displacements associated with the 1999 Chi-Chi, Taiwan earthquake, *Bull. Seismol. Soc. Am.*, *91*, 995–1012, doi:10.1785/0120000722.

Yu, S.-B., Y.-J. Hsu, L.-C. Kuo, and H.-Y. Chen (2003), GPS measurement of postseismic deformation following the 1999 Chi-Chi, Taiwan, earthquake, *J. Geophys. Res.*, *108*(B11), 2520, doi:10.1029/2003JB002396.

Zang, S.-X., Q.-Y. Chen, J.-Y. Ning, Z.-K. Shen, and Y.-G. Liu (2002), Motion of the Philippine Sea plate consistent with the NUVEL-1A model, *Geophys. J. Int.*, *150*, 809–819, doi:10.1046/j.1365-246X.2002.01744.x.

J. Angelier, OOV, port de la Darse, B.P. 48, F-06235 Villefranche-sur-mer, France.

K.-E. Ching and R.-J. Rau, Department of Earth Sciences, National Cheng Kung University, No. 1, University Road, Tainan 701, Taiwan.

J.-C. Hu (corresponding author), M.-H. Huang, and K.-C. Lin, Department of Geosciences, National Taiwan University, No. 1, Sec. 4, Roosevelt Road, Taipei 106, Taiwan. (jchu@ntu.edu.tw)

T.-C. Shin and C.-H. Tsai, Seismological Observation Center, Central Weather Bureau, 64 Gongyuan Rd., Taipei 100, Taiwan.

S.-B. Yu, Institute of Earth Sciences, No. 128, Sec. 2, Academia Road, Taipei 115, Taiwan.